Journal of Advanced Joining Processes 12 (2025) 100332

Contents lists available at ScienceDirect

Journal of Advanced Joining Processes

journal homepage: www.sciencedirect.com/journal/journal-of-advanced-joining-processes

Comparison of the economic efficiency and sustainability of two debonding processes for structurally bonded sills

Alex Jordan [a,*], Lucas Hermelingmeier [a], Julian Gilich [a], Gerson Meschut [a], Marco De Santis [b], Alexander Schlüter [b]

[a] Paderborn University, Laboratory for Material and Joining Technology (LWF), Warburger Straße 100, 33098, Paderborn, Germany
[b] Paderborn University, Sustainable Industrialization and Resilient Infrastructure (NIWI), Warburger Straße 100, 33098, Paderborn, Germany

ARTICLE INFO

Keywords:
Sustainable debonding
Structural adhesives
Sustainable joining technologies
Life Cycle Assessment (LCA)
Automotive repair process
Economically efficient debonding

ABSTRACT

In light of growing demands for resource efficiency and sustainability in vehicle engineering, the environmentally compatible separation of structural adhesive joints is gaining increasing relevance. This study presents a comparative analysis of two physically based debonding methods: the established hot-air process and a cryogenic cold process based on liquid nitrogen (LN_2). The primary objective is to assess the ecological impact and process-related sustainability of both approaches.

Experimental investigations were conducted on a component-representative triple-sheet structure that simulates common automotive flange joints. Thermal input was applied either by convective heating using a hot air gun or by direct cooling through a contact-based LN_2 tool. The resulting temperature profiles were recorded using spatially distributed thermocouples. Subsequently, the outer panel was selectively debonded to replicate a repair scenario, and the mechanical integrity of the remaining adhesive joint was evaluated through Mode I testing of l-shaped specimens. Process data served as input for an Life Cycle Assessment (LCA) according to DIN EN ISO 14,040.

The cryogenic method achieved a 40 % reduction in carbon footprint compared to the hot-air process (0.337 kg vs. 0.559 kg CO_2-equivalents), primarily due to its shorter process time and more efficient heat transfer. While the hot-air method's impact is mainly driven by electrical energy use, that of the cold method stems from cryogenic media consumption. Notwithstanding certain disadvantages in specific impact categories, the LN_2-based process exhibits a superior overall ecological performance and signifies a promising solution for repair- and recycling-oriented adhesive separation in structural vehicle applications.

Introduction

Adhesive systems enable efficient multi-material lightweight construction in various applications, especially in automotive body-in-white production, where the combination of high-strength steels, aluminium alloys, and fibre-reinforced polymer composites is of increasing interest (Bader et al. 2019). Compared to thermal and mechanical joining methods, adhesive bonding provides several benefits, such as homogeneous load distribution, improved damping behaviour, and corrosion resistance due to electrical insulation when bonding dissimilar materials (Stauber 2007). Additionally, adhesive joints offer considerable design flexibility, allowing for the integration of multifunctional components and the optimisation of vehicle structures during the design process. However, with the increasing prevalence of this joining technology, the significance of reversible separability for repair and recycling also increases (Statistisches Bundesamt 2018).

As legal and industry regulations tighten, the demand for product longevity, emphasising enhanced repairability and the reuse of materials and components at their end of life (EoL) has gained substantial importance (European Commission 2000). This shift has made disassembly a pivotal aspect of sustainable product development across the automotive industry and beyond (Lu et al. 2014). Incorporating reversible joining technologies during the design phase is crucial for the economic and ecological feasibility of material recovery and reuse. However, challenges arise when separating structural adhesive joints for repair or recycling purposes. For instance, in car body repairs, debonding must be performed carefully to prevent damage to adjacent structures. In these situations, the re-bondability of the previously

* Corresponding author.
E-mail address: jordan@lwf.upb.de (A. Jordan).

https://doi.org/10.1016/j.jajp.2025.100332

Available online 25 July 2025

bonded surface is essential. In contrast, recycling processes prioritise efficient disassembly and material separation over structural preservation. Therefore, identifying, sorting, and allocating separated materials into suitable recycling streams becomes a major priority. Nevertheless, structural adhesive bonds are often engineered for long-term durability and significant mechanical strength, which can complicate the targeted debonding necessary at the end of a product's life cycle.

Historically, adhesive joints were repaired using mechanical methods, such as cutting or peeling the adhesive layer, followed by the mechanical removal of the adhesive residue, for example by grinding or brushing, along with the application of repair adhesives (DVS 2012). In light of today's high-performance adhesives, however, alternative approaches are needed to weaken the adhesive layer prior to separation. Various technological approaches for debonding structural adhesive joints have been investigated. According to DIN/TS 54405 (DIN 2020), these methods can be categorised into mechanical, physical, and chemical processes, further differentiated by their respective mechanisms of action.

Targeted weakening of structural adhesive bonds is most effectively achieved through physical or chemical processes. Physical methods involve the input of thermal or electrical energy (DIN 2020). Heating the adhesive beyond its glass transition temperature causes temporary softening and reduces adhesion strength (Lu et al. 2014), which may lead to adhesive decomposition at higher temperatures (Banea 2019). Once softened, the bond can be detached with a secondary mechanical load. Traditional mechanical methods include cutting (Lu et al. 2014) and wedge-driven peeling (Bartley et al. 2023). This combined thermal-mechanical approach is currently employed in automotive repair but faces growing limitations due to the complexity and multi-material design of modern bonded joints. Additionally, controlling thermal input is challenging due to insufficient temperature monitoring capabilities within the bond line. Consequently, excessive heating can damage surrounding structures and undermine the joint's mechanical performance.

Cold debonding presents an alternative strategy by cooling the adhesive layer beneath its glass transition temperature, as researched and developed by Ditter (2020) and Chudalla (2024). This leads to embrittlement, reduces resistance to crack propagation, and restricts deformation during later mechanical separation (Bartley et al. 2023). Additionally, electrical techniques such as Joule heating (Leijonmarck et al. 2012), if the adhesive has been electrochemically modified (Leijonmarck et al. 2011), as well as impulse discharge methods that produce rapid material gasification (Inutsuka et al. 2023) are currently being explored.

Chemical approaches involve the integration of expandable agents (Concord 2021) or thermally responsive particles within the adhesive system (Borges et al. 2023), which induce volumetric expansion upon activation and disrupt the adhesive interface (da Silva et al. 2025). Additionally, the chemical structure of the adhesive can be modified using reversible reaction mechanisms, such as the Diels-Alder reaction (Sridhar et al. 2020), photochemical cleavage (Hohl et al. 2019), or external triggers like temperature (Heinzmann et al. 2016) or magnetic fields (Bandl et al. 2020). These adhesives are generally designed with tailored chemical or physical debonding capabilities. However, due to their low technology readiness level (TRL), chemical methods are mainly applicable in new product designs and are not yet suitable for widespread industrial use.

To date, the selection of debonding methods has been predominantly influenced by economic and technical criteria, including investment and operational costs, energy consumption, processing duration, and compatibility with existing production systems. Nevertheless, in complex supply chains, such as the automotive industry, suppliers are increasingly required to report environmental indicators, such as product-related CO_2 emissions, which have emerged as significant decision-making criteria in both product development and process selection.

Life cycle assessment (LCA) provides a methodologically standardised approach for quantifying environmental impacts. Within clearly defined system boundaries, relevant process data is systematically collected (Tillman et al. 1994) and evaluated to ascertain the environmental effects of materials, products, and production steps (Curran 2017). This enables a comprehensive analysis of environmental implications across the entire life cycle, encompassing both technological and socio-economic dimensions. The methodological framework is standardised in DIN EN ISO 14040 (ISO 2021a) and DIN EN ISO 14044 (ISO 2021b).

A variety of production processes have undergone LCA evaluation. Gialos et al. (2018) analysed the impact of laser-welded components in aircraft applications, Khripko et al. (2013) conducted a product carbon footprint (as part of an LCA) for product products, and Gagliardi et al. (2019) investigated joining processes in hybrid structures. Numerous studies have been conducted on various forms of welding, including arc welding (Sangwan et al. 2016), gas welding (Shrivastavaa et al. 2015), laser welding (Yilbas et al. 2020), and friction stir welding (Bevilacqua et al. 2017). In the field of adhesive bonding, Favi et al. (2021) examined several surface pretreatment methods, while Maciel et al. (2017) performed an LCA of solvent-, water-, and powder-based polyurethane adhesives. Sato et al. (2021) conducted a comparative analysis of the ecological impact of adhesive bonding, with particular attention given to the debonding methods as delineated by DIN/TS 54405. The environmental impacts of adhesives are primarily attributed to the three main mechanisms, greenhouse gas emissions, release of toxic substances, and utilisation of finite resources.

In summary, existing sustainability-focused studies principally address the joining process and associated pre- and post-processing steps. Conversely, the ecological assessment of debonding processes remains unexamined mainly in quantitative terms. The current literature has predominantly focused on the technical feasibility of the process and its subsequent classification. While Goodenough et al. (2023) evaluated debonding technologies for fibre-reinforced polymers, a systematic environmental assessment, including quantification of material and energy flows, impact analysis, and comparative evaluation, has not yet been conducted for structural adhesive joints in an industrial context.

This study aims to enhance the traditional technological evaluation of debonding methods by incorporating ecological factors into the selection process. It involves analysing process duration, evaluating the potential reusability of debonded components, and identifying potential resource savings in repair scenarios. Furthermore, the study identifies key environmental impact drivers within the debonding processes to uncover optimisation opportunities for reducing current CO_2 emissions. The focus is on both established and innovative methods for debonding structural adhesive joints, assessing their applicability in the contexts of vehicle repair and recycling. The analysis utilises experimental investigations with component-representative demonstrators. The subsequent LCA follows the guidelines set forth by DIN EN ISO 14040 (ISO 2021a), DIN EN ISO 14044 (ISO 2021b), the International Reference Life Cycle Data System (ILCD) guidelines (Joint Research Centre 2010), and the Handbook on Life Cycle Assessment (Guinée et al. 2002).

Methods

The present study aimed to compare a traditional warm debonding method with an innovative cold debonding method, which is fundamentally based on the proven mechanism introduced by Chudalla (2024) but adopts LN_2 as a substitute medium to pursue more efficient and targeted approaches. It focused on their processing efforts, the effects on surrounding structures, and the environmental impacts resulting from the processes and any required reworking. Initially, temperature change rates were measured using both stationary positioning and oscillating movement patterns of the thermal tools in the adhesive layer intended for debonding. Subsequent analyses calculated

the lead times for initial temperature changes in the profile section and determined the holding times needed to achieve the target temperature. These measurements laid the groundwork for the debonding tests. Both methods were then employed to detach the cover sheet from the demonstration structure. To evaluate the environmental impact, the duration of the debonding tests and the associated material and energy consumption were carefully documented. The recorded data were used in an LCA of the debonding methods. Subsequently, l-samples were extracted from the remaining demonstration structures to assess how the separation process affected the residual load-bearing capacity of the second adhesive layer. This analysis facilitated the estimation of potential repair or maintenance costs.

Specimen configuration and adhesive system

To simulate realistic disassembly scenarios and facilitate ecological and economic evaluation of repair strategies, a defined specimen configuration was employed, which builds upon the methodology presented by Bartley et al. (2023). The triple-sheet configuration, illustrated in Fig. 1, consists of an outer skin (CR4+*Z*), a cover sheet (22MnB5 PHS), and a hat profile (HX340LAD), replicating the functional composition of structural body-in-white assemblies. The outer panel represents a typical contour part, such as a side sill, while the cover sheet and hat profile mimic reinforcement and inner structural elements, respectively. The mechanical properties of the individual steel sheets are listed in Table 1.

The arrangement facilitates an evaluation of various debonding techniques, emphasising the reduction of thermal and mechanical impacts on the outer panel. Additionally, the geometry allows for the assessment of the residual bond line integrity between the cover sheet and the hat profile after disassembly. The experimental setup, along with the thermocouple configuration within the adhesive layer, is depicted in Fig. 1.

The adhesive used in this study, SikaPower®−533 MBX, is a one-component, heat-curing epoxy adhesive commonly applied in automotive body-in-white construction. It is a high-strength structural adhesive specifically designed and qualified for high-crash resistance and mixed-material bonding applications, enabling the reliable joining of dissimilar substrates. The key technical properties of the adhesive are presented in Table 2.

Table 1
Mechanical properties of the steels used in this study, determined in (*Bartley et al. 2023*).

Steel designation	EN steel number	Thickness (mm)	E-Module (GPa)	Rp0.2 (MPa)	Rm (MPa)	A50 (%)
CR4	1.0963	0.7	196	161	302	46.4
HX340LAD	1.0933	1.5	208	358	456	29.4
22MnB5	1.5528	1.8	206	1153	1531	4.8

The specimens were fabricated under controlled laboratory conditions. The adhesive was manually applied to ensure a 0.3 mm bond line, using glass beads for consistency with automotive standards. The effective bond area between the cover sheet and hat profile measured 12.5 × 500 mm. To ensure reproducibility and facilitate the comparison of heat transfer data across experiments, positioning tolerances of the steel sheets were maintained at ±1 mm in the longitudinal direction (specimen length) and ±0.2 mm in the transverse direction (flange width) for all specimens.

To enable an in-depth characterisation of the thermal behaviour, specially instrumented specimens were equipped with 20 Type T thermocouples, centrally embedded within the adhesive layer as shown in Fig. 1. The thermocouples were arranged in two longitudinal rows of ten sensors each, spaced at 50 mm intervals, while the outer two sensors were positioned 25 mm from the edge of the metal sheets, thereby providing detailed spatial resolution of the in-situ temperature distribution during the heating and cooling experiments.

The selected spacing of 50 mm was intentionally chosen to ensure methodological consistency with the setup described in (Bartley et al. 2023), thereby facilitating comparative evaluation. This decision reflects the typical geometries of cooling tools used in both industrial and research applications, particularly those designed for bonded flanges, which generally feature overlap lengths ranging from 85 to 100 mm. The chosen sensor arrangement thus enables a representative characterisation of the thermal profile within the adhesive layer. With the defined spacing of 50 mm, the local cooling behaviour can be captured with high spatial resolution and in close alignment with various tool configurations.

The adhesive curing was conducted in a laboratory convection oven set to 180 °C. The thermal cycle was meticulously controlled and

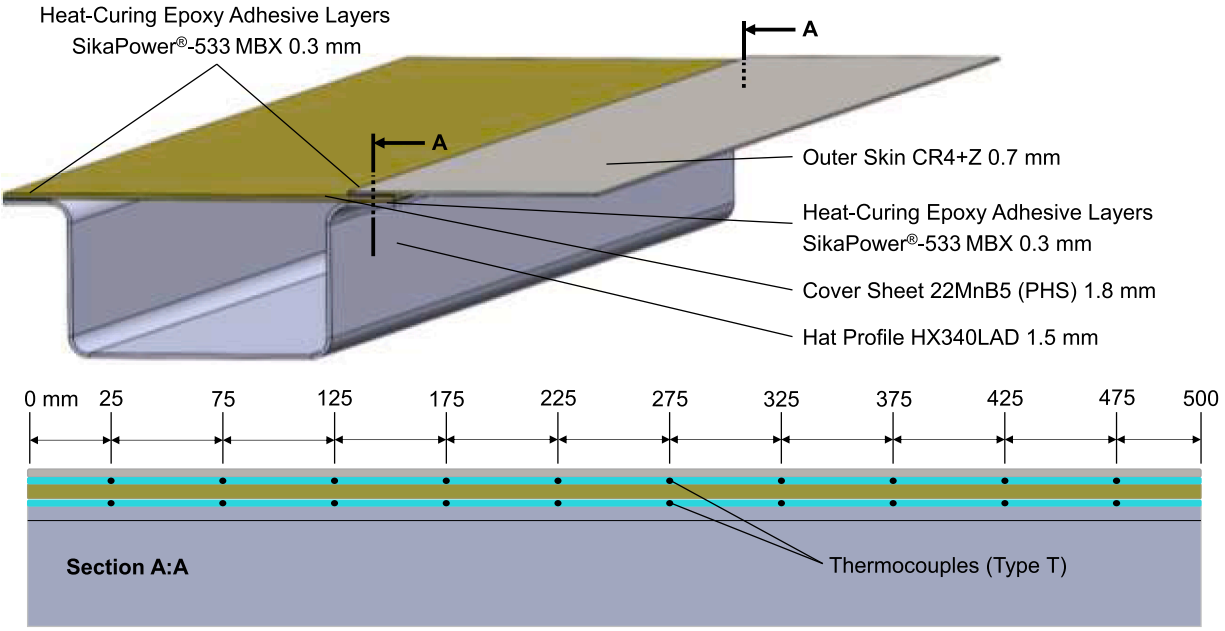

Fig. 1. Component-representative specimen geometry used for the debonding assessment.

Table 2
Technical properties of the adhesive used in this study, taken from (Sika 2011).

Adhesive	Chemical base	Standard curing cond. [A]	Tensile lap-shear strength [B/C/D] (MPa)	T-peel strength [B/E/F] (N/mm)	Elongation at break [G] (%)	E-Module [G] (MPA)
SikaPower® 533 MBX	Epoxy hybrid	30 min at 180 °C	27	20	20	850

A) substrate temperature.
B) steel, HDG, H420, 1.2 mm.
C) bondline thickness 0.2 mm.
D) ISO 4587.
E) bondline thickness 0.3 mm.
F) ISO 11,339.
G) ISO 527.

systematically recorded using a multi-channel thermogravimetric analyser. The temperature of the specimen was monitored with a Type K thermocouple, positioned at the centre of the outer flange area of the hat profile and secured with a magnet. This method allowed for the accurate verification of the thermal profile, ensuring consistent cross-linking present in all samples. Curing was maintained for 30 minutes after the hat profile reached the target temperature of 180 °C.

Extended specimens for the investigation of thermal effects on the overall structure

To assess the thermal impact of the thermal debonding processes on adjacent structural components and retained adhesive layers, additional specimens were extracted from the component-representative configuration shown in Fig. 1, following the complete debonding of the CR4 outer panel. These specimens consist of modified l-shaped samples subjected to Mode I loading, as illustrated in Fig. 2. Precisely ten l-shaped specimens can be derived from a single debonded structure, thereby facilitating a spatially resolved analysis of the thermal effects across the adhesive joint.

This test series aim to identify any potential reductions in the bond strength of the underlying adhesive layer, which is designed to retain its functionality following disassembly. To achieve this, reference specimens were prepared using identical bonding procedures and curing conditions but without subsequent exposure to debonding thermal cycles, thereby representing the original adhesive joint properties.

Debonding methodology and process definition

The debonding methods examined in this study are based on the same physical principle, whereby the mechanical force required to debond the adhesive layer is significantly reduced through a targeted and temporary alteration in the adhesive layer temperature. Both investigated methods differ in their mechanisms depending on the type of thermal influence: while warm debonding involves heating the adhesive beyond its glass transition temperature ($T_g \sim 180$ °C) and, in some cases, inducing thermal degradation (> 200 °C), cold debonding achieves embrittlement by reducing molecular mobility through controlled subcooling (e.g., < -60 °C) using liquid nitrogen, thereby weakening the adhesive interface (Bartley et al., 2023). In both methods, mechanical separation is initiated using an Einhell TC-PC 45 pneumatic chisel hammer, subsequently referred to as “chisel hammer” or “hammer”, operated at a system pressure of 7 bar. The thermal tools applied in this investigation serve as representative examples. The physical effects of both methods may also be achieved using other comparable tools or process equipment. The experimental setup is illustrated in Fig. 3 and described in more detail in the following section. For all debonding experiments, specimens were securely clamped onto a welding table to replicate the structural stiffness and boundary conditions of a vehicle body during repair operations. This setup ensures that the applied forces and structural responses are representative of real-world automotive applications. Prior to each experiment, the thermal devices were brought to their respective target operating conditions to eliminate start-up variations from the measurements.

Warm debonding

For Warm Debonding, a hot air device of type LHS 21S SYSTEM from Leister (8) was employed. This system operates with compressed air at an overpressure of 1 bar combined with electrical energy. The temperature of the emitted process air can be precisely adjusted on the unit, reaching a maximum of 650 °C. To ensure realistic conditions that reflect standard practices in automotive body shops, and considering the observation that commercially available hot air devices typically attain maximum outlet temperatures ranging from 550 °C to 650 °C (Hutchinson et al. 2016), a constant air temperature of 550 °C was maintained for all test series. To ensure reproducible thermal boundary conditions, the hot air unit was securely mounted on a stand, maintaining a fixed nozzle distance of 25 mm from the adhesive flange surface intended for separation. Following the stabilisation of the air stream at the set point temperature of 550 °C, the hot air was directed towards the adhesive flange (see Fig. 3), initiating forced convection between the heated airflow and the metallic outer sheet. In practical applications, it is noteworthy that a hot air gun does not focus on a single flange area in a fixed position. Instead, it is operated with rotational movements across the flange to heat a more extensive area (Hotairtools 2024) uniformly.

As the bonded flange region was subjected to elevated temperatures, the pneumatic chisel hammer (4) was strategically positioned at the edge of the flange and briefly activated to create a controlled notch within the adhesive layer. Upon reaching the requisite temperature of the adhesive, the chisel hammer was continuously actuated and guided along the bonded flange. The debonding of the adhesive bond was

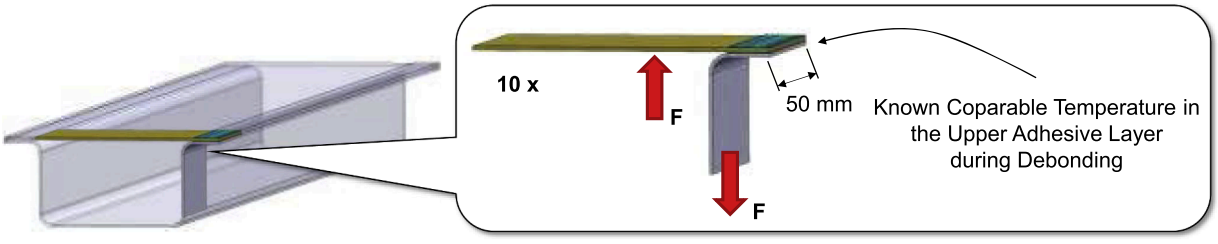

Fig. 2. Extended Mode I specimen geometry obtained from the debonded component specimen.

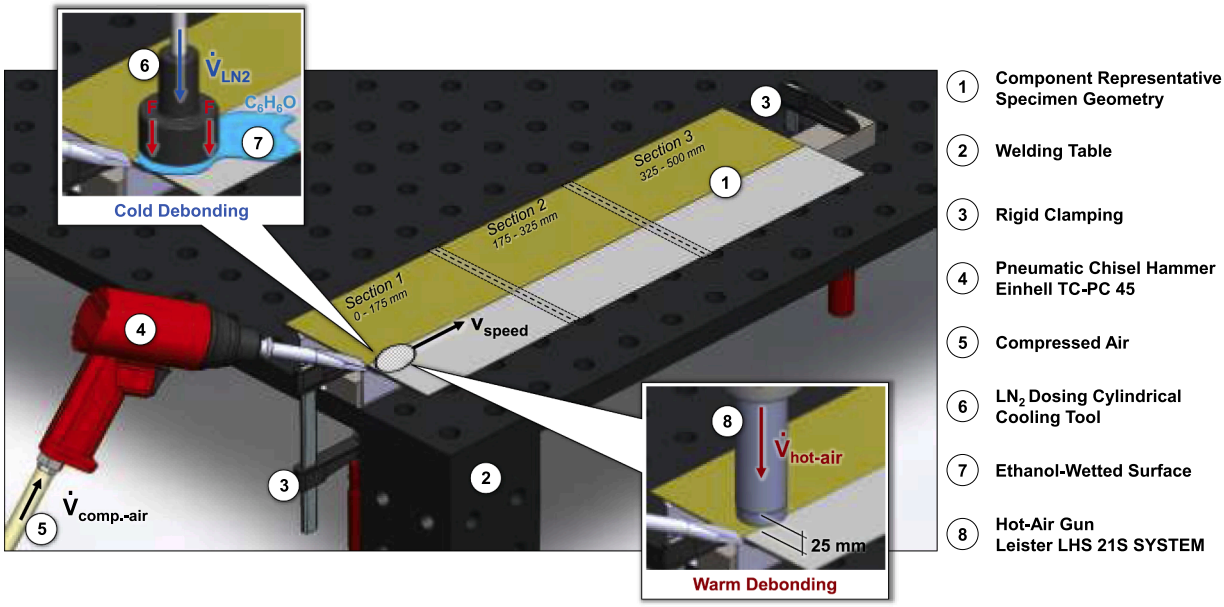

Fig. 3. Test configuration for comparative analysis of warm and cold debonding methods.

achieved through the application of oscillating, percussive mechanical force directed at the thermally weakened adhesive layer. This repetitive cycle was executed until the adhesive bond between the outer sheet and the reinforcement plate was entirely debonded.

Cold debonding

For cold debonding, LN_2 serves as a heat-extraction medium, lowering the temperature of the adhesive layer. The LN_2 is supplied from a Dewar vessel via a micro-dosing pump through a flexible line to a custom-designed cooling tool, which is schematically illustrated in Fig. 4.

The cooling tool is fitted with a copper mesh insert to minimise thermal contact resistance between the flange surface and the cooling element, as well as to extend the residence time of LN_2 on the cooled flange area. To mitigate the Leidenfrost effect, which significantly degrades heat transfer efficiency by forming an insulating vapour layer (Zhong et al. 2017), ethanol (C_2H_6O) with a purity of 95 vol. % is also applied directly onto the flange (7). The resulting mixture of LN_2 and ethanol facilitates a uniform wetting of the surface, thereby promoting efficient heat transfer from the flange to the cryogenic medium, primarily via natural convection. The methodological basis for cold debonding is grounded in the approach delineated by Bartley et al. (2023), albeit with a differentiation in the cooling medium employed. Given its laboratory nature, operations involving the movement of the cooling head, operation of the chisel hammer, and ethanol application are executed manually.

During the initial phase of cooling, the pneumatic chisel hammer is positioned at the edge of the flange and briefly activated to create a notch within the adhesive bond. The chisel tip effectively propagates the crack front through the adhesive joint by means of impulse-driven force. Should crack propagation experience deceleration due to insufficient localised subcooling, ethanol is reapplied to the surface of the bonded flange in advance of the chisel tip, and the cooling head is subsequently repositioned. This systematic sequence of localised cooling and mechanical separation is reiterated until complete debonding of the adhesive bond between the outer and stiffening sheet is achieved. Upon conclusion of the procedure, the components are allowed to warm to ambient temperature, wherein any excess LN_2 and ethanol fully evaporate, leaving no residual process media on the parts post-debonding.

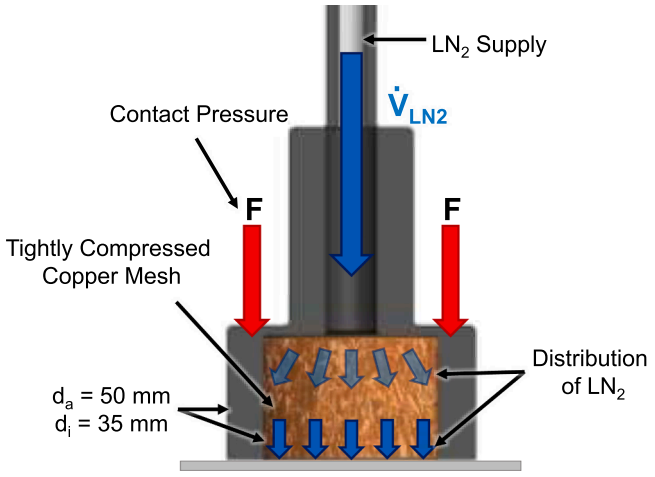

Fig. 4. Design and operating principle of the LN_2-dosing cylindrical cooling tool.

Experimental design and measurement setup

In order to evaluate the impact of the investigated debonding methods on the structural integrity of the adjacent components and to gather all relevant measurement data necessary for an LCA, three distinct experimental test series were carried out. The first series focused on measuring the temperature within the adhesive layer designated for separation, as well as in the lower adjacent adhesive layer, based on the various thermal input methods employed. From this data, the lead time and total process durations for both release methods were derived. A total of five test runs were conducted for each debonding methods. The second test series employed both methods on the component-representative specimen geometry, capturing the resulting process durations along with the associated material and energy consumption. In the third test series, modified l-shaped specimens were subjected to destructive tensile testing. The resulting force-displacement curves enabled the calculation of the residual energy absorption capacity of the adhesive layer, thus providing insight into the condition of the remaining joint and the adjacent structure following the debonding process.

Temperature measurement

Two distinct types of movement for the temperature-modifying device were examined within this experiment. During the first trial, the apparatus was positioned at the initial thermocouple point ("25 mm"), aligned with the cover plate, and subsequently shifted to the next thermocouple position when the designated target temperature was achieved. This sequence was replicated until the final thermocouple location was reached. The target temperature for the adhesive layer, situated between the outer skin and the stiffening cover sheet, was set at 200 °C for the warm method and −70 °C for the cold method. Throughout the experiment, the temperature across all 20 thermocouples was monitored at a frequency of 1 Hz.

The distances from the temperature-altering device to the flange set for separation were consistent with those measured during the stationary assessments. The real-part-like sample was segmented into three overlapping sections based on its measurement positions. The first section spanned measuring positions from "25 mm" to "175 mm", while the second section extended from "175 mm" to "325 mm". Thus, sections 1 and 2 overlapped at "175 mm". Similarly, the overlap area between sections 2 and 3 was defined by the position "325 mm". This designed overlap was instrumental in ensuring the requisite temperature change could be engendered in those areas as well.

The axis of the temperature-altering device played a crucial role in determining the swivelling movement. The respective device was manually manoeuvred at an approximate speed of 1 cm/s within each section. Upon recording the necessary temperature at least at one of the measurement points, the temperature alteration continued into the subsequent section. This procedural cycle was reiterated until the requisite temperature was confirmed across all three sections.

Investigation of the influence on the surrounding structure

The assessment of thermal effects on the surrounding structural components was conducted by determining the residual mechanical strength of the l-shaped specimens described in Section 2.1.1. The test method adheres to the general principles of DIN EN 1464 (DIN 2010) and DIN EN 1465 (DIN 2009) in a modified configuration, reflecting the boundary conditions illustrated in Fig. 5.

In the test setup, the originally press-hardened cover sheet is rigidly clamped, thereby restricting the degrees of freedom in the Z and Y directions. Sliding bearings permit translational movement along the X-axis, preventing the development of complex stress states induced by tensile loading in the Z-direction. Therefore, a predominantly peel-type loading is applied to the adhesive joint, analogous to the roller peel test defined in DIN EN 1464 (DIN 2010a). Elastic spring-back caused by the applied force could not be fully suppressed, because of the one-sided clamping. Consequently, the adhesive-specific energy absorption could not be directly derived from the force-displacement measurements. However, given that all specimens were cut to identical dimensions and the clamping setup exhibited high reproducibility, the total deformation energy was calculated instead. This value accounts for both the elastic deformation of the clamped steel components and the plastic deformation of the adhesive layer up to failure. Due to the consistent manufacturing and boundary conditions, the elastic contributions can be considered constant across all tests, enabling a comparative interpretation of adhesive performance. The Zwick Z1486 tensile testing machine operated at 10 mm/min crosshead speed.

Results –process parameters

Removal rate and resulting deformation

Process lead times were determined from temperature measurement data to ensure reproducible debonding initiation. The results of the first test series revealed lead times of 45 seconds for warm debonding and 25 seconds for cold debonding. The 20-second difference is attributed to the respective target temperatures. While the adhesive layer must be heated to at least 180 °C for warm debonding, it needs to be cooled below -65 °C for cold debonding. Since both conditions are reached from a reference temperature of 20 °C, this corresponds to temperature variations of at least 160 K and 85 K, respectively. The device-dependent lead times thus correlate with the necessary thermal gradients. Both the lead time and the temperature difference for warm debonding are approximately twice as high as those for cold debonding. Heating and cooling rates also depend on the quantity and efficiency of the energy or medium used in the process and are examined in detail in Section 3.2.

It is important to consider the boundary conditions when interpreting these findings, as the thermal capacity of the specimen is significantly influenced by the materials used, the adhesive system, the geometry, and the ambient environment. In particular, the time required to reach the effective debonding temperature is determined by the thermal gradient between the heating or cooling medium and the substrate, making any absolute process durations highly specific to the applied setup. Therefore, a direct transfer to other structures is not readily applicable. Nonetheless, a comparison of total debonding durations shows that the cold method can be applied nearly twice as fast to the present specimen geometry as the warm method, which simulates

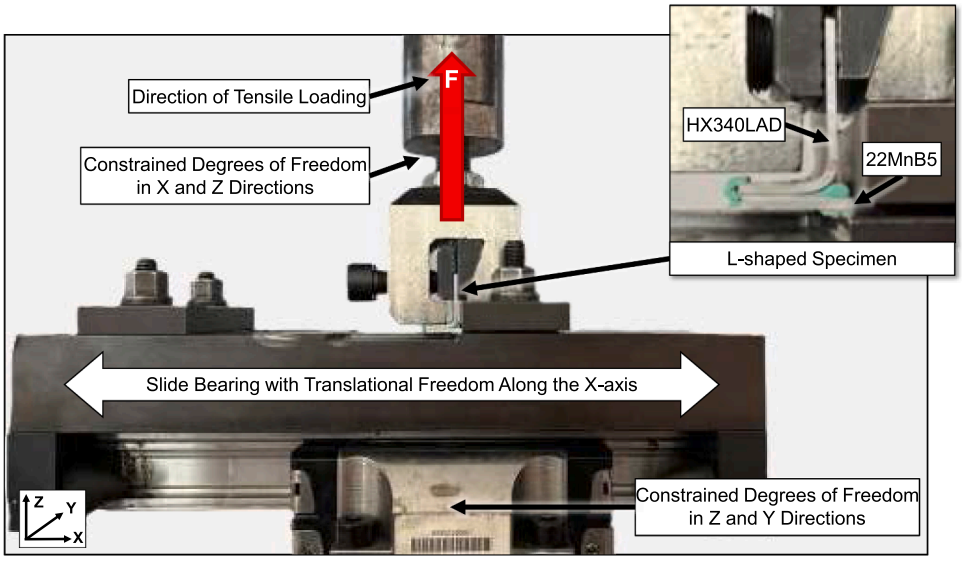

Fig. 5. Test setup for mechanical evaluation of l-shaped specimens extracted from debonded structures.

current practice in automotive repair. This ratio is also reflected in the total separation times shown in Fig. 6. While warm debonding required an average of 224.6 seconds to fully separate the outer sheet, the cold method achieved complete separation in an average of 131.6 seconds. When normalised to the underlying profile length, average debonding speeds of 173.91 mm/min for the warm method and 353.57 mm/min for the cold method are obtained. This indicates that the cold method achieves more than twice the process speed of the warm method, highlighting its efficiency advantage. The accelerated debonding contributes to reduced overall thermal exposure, as shorter temperature application durations are typically associated with higher energy efficiency. However, it is important to note that this calculation excludes the initial lead time. Since this lead time is only relevant at the beginning of the process, its relative impact diminishes as the flange length increases, thereby reducing its proportion of the total debonding time. The assessment of process performance, especially with regard to potential automation, should therefore focus on the stable debonding rate rather than isolated initiation delays. Nevertheless, as previously discussed, this component-specific lead time remains a relevant parameter when comparing the practical applicability of the two methods.

Another contributing factor lies in the process characteristics. While the LN_2-ethanol mixture in the cold method remains on the flange surface and extracts heat through evaporation, the heated air in the warm method is continuously displaced by the airflow itself. As a result, the residence time of the heated air is shorter, impeding complete heat transfer to the flange and ultimately prolonging the debonding process.

The relative standard deviation of the total debonding duration was found to be higher for the warm method (17.90 %) as compared to the cold method (14.26 %). Nevertheless, both values are at a comparably high level, which can be attributed to the inherently manual execution of the process. Specifically, the involvement of two operators introduces a degree of variability, underscoring the importance of operator experience in optimising performance outcomes. This observation signifies potential improvements in both debonding methods, as the duration of the process could be minimised through a precisely calibrated and automated debonding setup.

During the experiments, it became apparent that adherence to the specified lead time was crucial for initiating a crack within the adhesive layer. Distinct deformation characteristics were observed in the debonded outer sheets between the two methods. The outer sheets processed via warm debonding exhibited notably greater curvature compared to those separated using the cold method, which showed predominantly straight, less deformed areas.

Fig. 7 illustrates representative crack propagation patterns observed during equivalent time intervals following chisel activation. The video images suggest that under similar operating pressures, the chisel penetrates more extensively into the separating joint during cold debonding compared to the warm method. This observation may indicate enhanced crack advancement in the embrittled adhesive, potentially allowing the chisel to progress with reduced mechanical resistance.

Video analysis revealed preliminary indications of differing crack propagation lengths between the methods. In warm debonding, crack advancement appeared to be limited to zones approximately corresponding to the heated area (estimated 25–30 mm), requiring continuous tool repositioning. In contrast, cold debonding suggested crack propagation lengths potentially extending 60–80 mm beyond the cooling head position after each chisel impact, indicating possible autonomous crack advancement through the embrittled adhesive layer.

Based on these visual observations and considering findings from previous studies on adhesive embrittlement (Chudalla 2024), it is hypothesised that the increased brittleness of the adhesive during cold debonding facilitates more extensive crack propagation lengths. This presumed mechanism could explain the reduced sheet deformation observed in cold debonded specimens, as rapid crack advancement may minimise the mechanical load transfer to the outer sheet. The mechanics of crack initiation in cold debonding appear to differ fundamentally from the propagation phase. While embrittlement may increase the force required for initial crack nucleation (preliminary measurements suggest approximately 15–20 % above warm debonding values), the subsequent crack propagation appears to occur with significantly reduced resistance. The initial higher force requirement seems to be quickly compensated by the rapid crack propagation through the brittle adhesive matrix, potentially resulting in the observed energy reduction. This apparent contradiction could be explained by the two-phase nature of

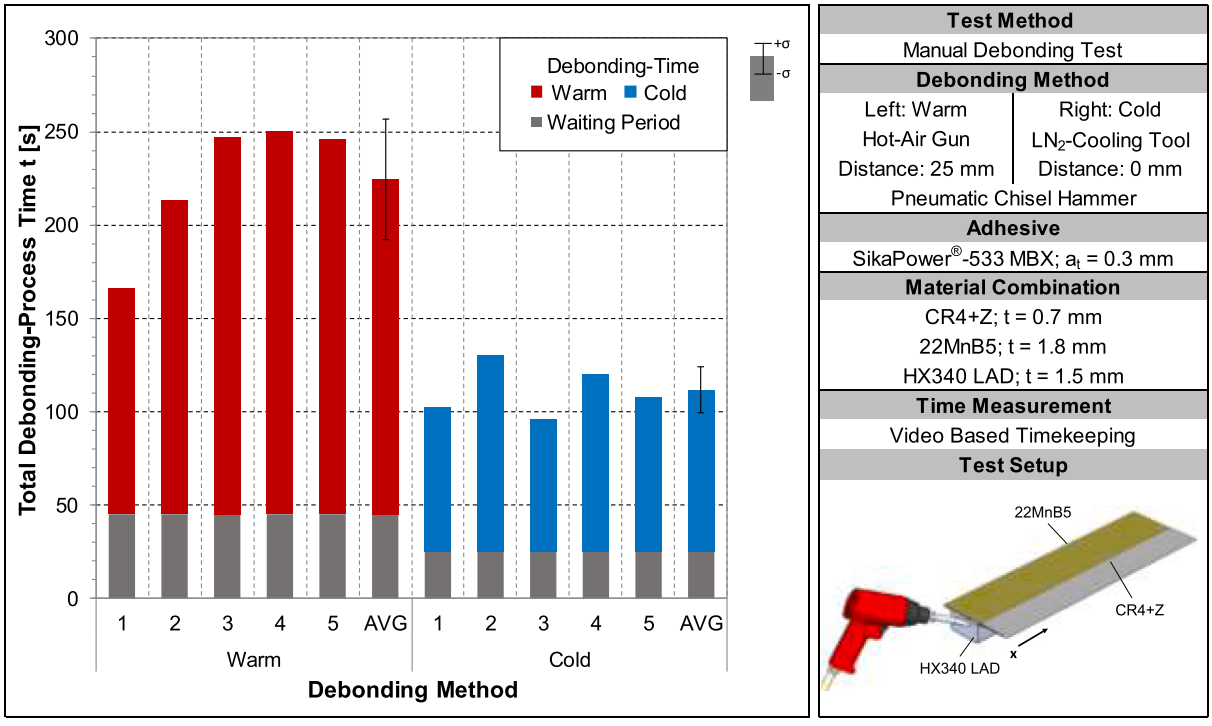

Fig. 6. Total debonding process times depending on the debonding method used.

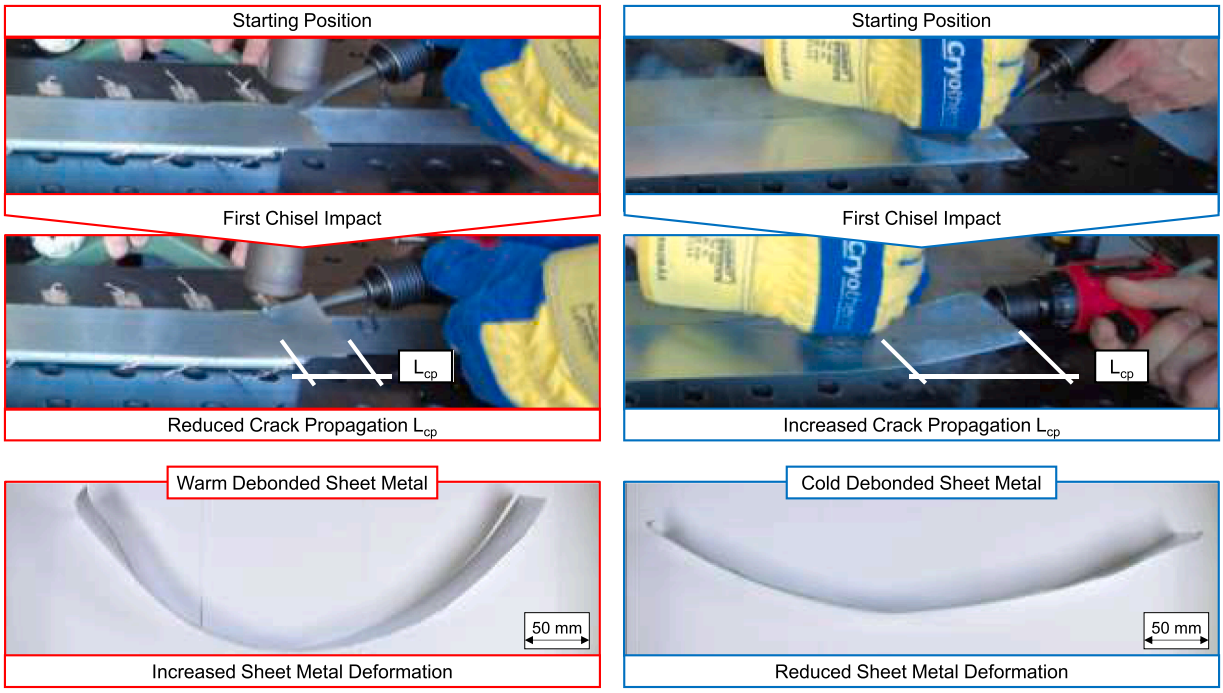

Fig. 7. Representative crack propagation patterns and resulting sheet deformation observed during equivalent time intervals following chisel activation for both warm and cold debonding methods.

the debonding process: While crack initiation may require higher instantaneous force in the cold method (due to increased material strength), the crack propagation phase appears to be drastically accelerated due to reduced fracture toughness. However, these observations require further investigation through quantitative crack measurement techniques and additional optical analysis methods to establish definitive correlations between thermal conditioning, crack propagation mechanics, and resulting sheet deformation. The current findings represent preliminary indications that warrant more detailed mechanical analysis in future studies.

Properties of the adjacent adhesive layer

A further critical aspect to consider when comparing these two debonding methods is the mechanical residual properties of the adjacent adhesive layer. Given that warm debonding is the prevailing method in the context of repair applications, a predictable mechanical response of the surrounding structure is imperative for ensuring reliable joint

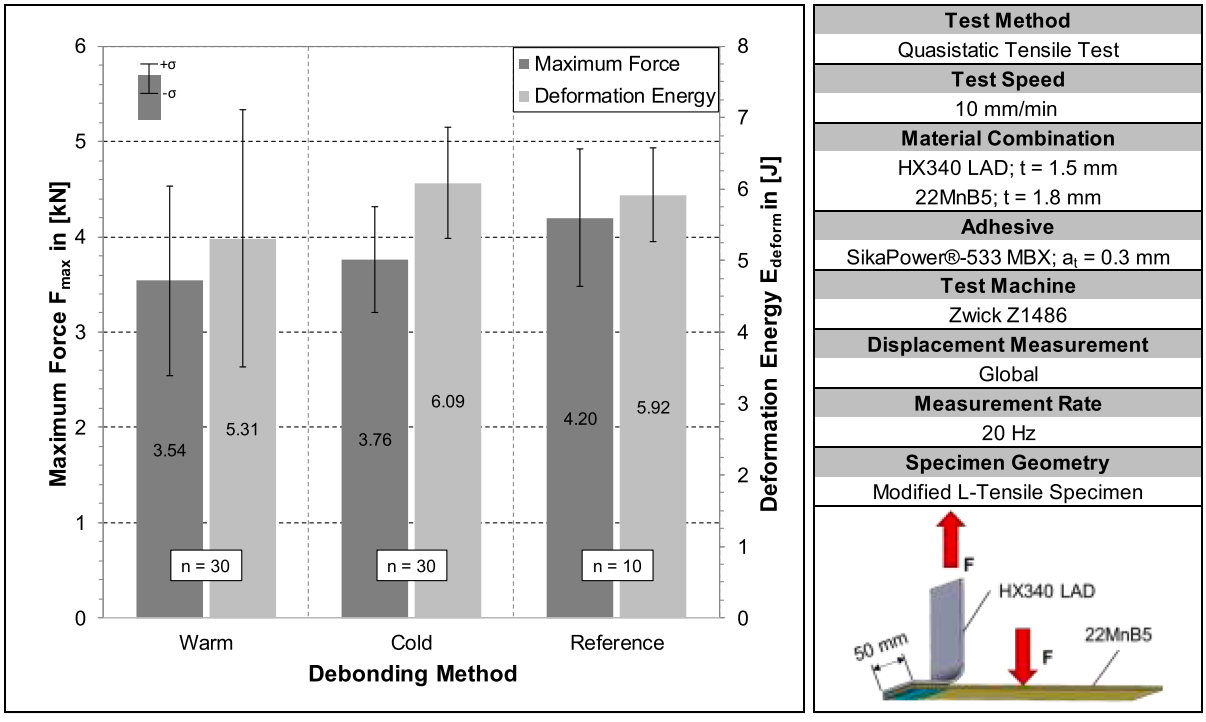

Fig. 8. Average values of maximum force and deformation energy of the modified l-Tensile Specimen in relation to the debonding method.

performance in the post-repair phase. The interdependence of mechanical properties on debonding duration, particularly in conjunction with the high variability of process times, poses a risk to the performance assurance of repaired structures. Therefore, modified l-shaped specimens have been tensile tested to obtain preliminary insights into the mechanical performance of the surrounding adhesive bonds. These bonds may have been subjected to thermal and mechanical loads due to the preceding debonding processes.

Fig. 8 illustrates the mean values of maximum force and deformation energy as a function of the debonding methods. The results from the reference specimens show an average maximum force of $F_{max,R} = 4.2$ kN and a total deformation energy of $E_{deform,R} = 5.92$ J. In terms of the specimens from the warm-debonded profiles showed an average maximum force of $F_{max,W} = 3.54$ kN and a total deformation energy of $E_{deform,W} = 5.31$ J whereas the specimens from the cold-debonded profiles showed an average maximum force of $F_{max,C} = 3.76$ kN and a total deformation energy of $E_{deform,C} = 6.08$ J respectively. Although the average values differ in respect to the foregone thermal load, the standard deviation in all parameter sets is so high, that the average values are within the standard deviations of the other specimen groups. Consequently, no clear correlation between debonding method and residual mechanical performance can be seen based on these results.

Despite the considerable number of specimens that were tested, the relative standard deviation in maximum force and total deformation energy is considerably higher for the warm debonding method (28.07 % and 33.98 %) in comparison to the cold debonding method (14.76 % and 12.76 %). The standard deviation from the reference specimens (17.11 % and 11.07 %) is comparable to the standard deviation from the results from the cold debonding method. This discrepancy in outcomes can be attributed to the manual fabrication of the profile specimens. In this experiment, the quantity of adhesive applied exerts a substantial influence on the degree of squeeze-out observed for each specimen. As the profile specimens were designed to replicate a genuine adhesive application, and the inner corners of the hat profiles were not accessible for the removal of excess adhesive, the amount of squeeze-out could not be controlled. This issue is particularly salient when testing a specimen with peel-dominated loading, where the excess adhesive impacts the maximum force, F_{max}, which is observed during crack initiation in the bond. This is due to the fact that the line of force and line of adhesion are not perpendicular to each other. The standard deviations are also affected by this circumstance due to the linkage between maximum force and total deformation energy. Fig. 9 shows representative images of the fracture surfaces of the modified l-specimens, depending on the previously applied debonding method.

All specimens exhibited cohesive or nearly substrate cohesive failure towards the stiffening sheet. The amount of residual adhesive was comparable across all test series, indicating that the impact of expelled adhesive on the standard deviation of the mechanical properties can largely be ruled out. Since both debonding processes aim at a temporary alteration of the adhesive layer condition while leaving surrounding bonds unaffected, this outcome is to be considered positively in terms of process selectivity. The absence of cracks, burn marks, or other visible defects indicate that the debonding methods did not cause unintended damage to adjacent areas. Nevertheless, identifying the precise cause of the elevated standard deviation in the results from the warm method require further microscopic analyses and additional testing.

Temperature distribution within the adhesive layers

In order to assess the thermal implications of the debonding processes on the adhesive layer and its surrounding components, a comprehensive analysis of the spatial and temporal temperature distribution within the joint structure was conducted. The in-situ measurements obtained from the embedded thermocouples deliver an intricate profile of the thermal loading during both the heating and cooling phases.

Stationary thermal profiles: warm vs. cold debonding

The temperature profiles presented were recorded during thermal loading of the component using the tools underlying the warm and cold debonding methods, without initiating adhesive separation. Each diagramme displays the temperature progression (y-axis) over time (x-axis). The colour-coded curves correspond to the individual thermocouple measurings distributed along the adhesive flange. The analysis is initiated with the evaluation of the stationary test series, in which the thermal device is advanced stepwise from one measurement point to the next (see Fig. 10). Progression to the subsequent position only occurs once the predefined target temperature of 200 °C for the warm method or −70 °C for the cold method has been reached at the current location.

For the warm debonding method, approximately 100 seconds are required to heat the upper adhesive layer at the first measurement point (solid black line) to the target temperature of 200 °C. As a result of convective heat transfer, adjacent measurement points along the flange are progressively preheated, leading to a stepwise acceleration of the heating process. Complete heating of the adhesive flange is achieved after 580 s, at which point the initially heated regions have cooled to approximately 50 °C.

It is also evident that the temperature in the lower adhesive layer (dashed lines) rises to 150–160 °C, significantly exceeding the typical temperature tolerance of approximately 80 °C for structural adhesives used in automotive applications. As a result of the system's thermal inertia, the lower adhesive layer is exposed to a critical thermal load over an extended period, with an average peak temperature of approximately 143 °C, which must be regarded as detrimental to its functional integrity.

In contrast, the analysed cold debonding method achieves the target temperature of −70 °C at the first measurement point after just 26 s. The subsequent points reach this temperature successively at intervals of 10–18 s. Unlike the warm debonding method, the temperature in the lower adhesive layer remains above the critical adhesive operating temperature of −40 °C at all times. This is due to the significantly higher efficiency of heat extraction during cold debonding and the faster subsequent temperature equalisation, demonstrating a considerably higher achievable cooling rate compared to the heating rate. The total process duration for cold debonding in this configuration is 153 s. In addition to the overall process duration, a significant difference between the two

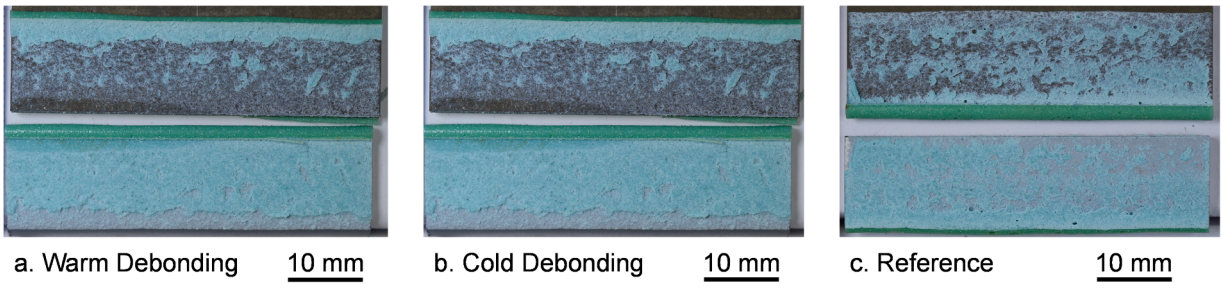

Fig. 9. Representative fracture images of the second adhesive layer following tensile tests on the modified l-samples, depending on the prior debonding method.

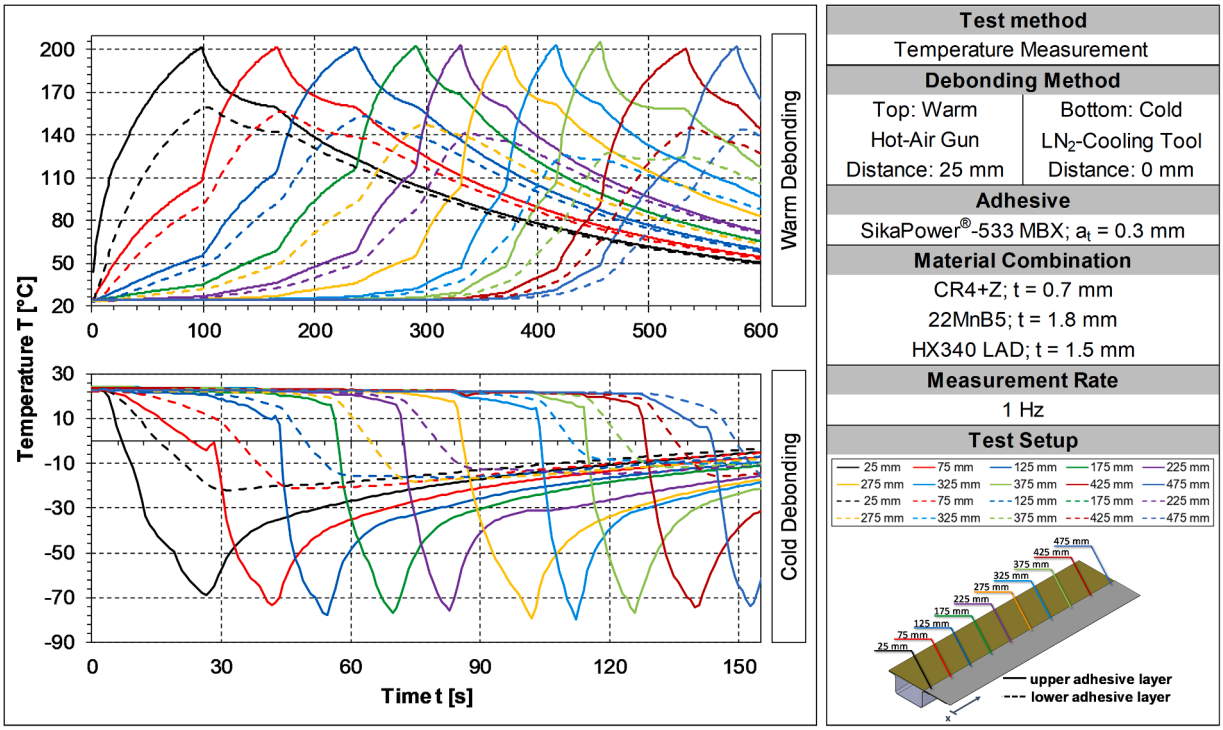

Fig. 10. Process-induced temperature changes within the adhesive layers during warm and cold debonding.

debonding methods lies in the thermal rate of change. The heating rate, defined as the convective energy input into the structure via the hot air gun, was noticeably lower than the cooling rate achieved through thermal extraction via direct LN_2 contact. This asymmetry reflects the physical efficiency of thermal transfer mechanisms. While heating relies on gradual energy accumulation, cooling by LN_2 permits an immediate and rapid withdrawal of thermal energy. Beyond the generally faster process execution, this leads to enhanced thermal recovery to ambient temperature and improved process control.

Oscillating thermal profiles: practicality and limitations

The oscillating test procedures detailed in Supplementary Material 1 (warm debonding) and Supplementary Material 2 (cold debonding) do not result in any measurable acceleration of the heating or cooling processes. Due to the oscillating motion of the hot air gun across the specified three flange sections, >350 seconds were required per section, resulting in a total process time exceeding 1000 s. During this extended period, the lower adhesive layer was once again subjected to critically high temperatures surpassing 150 °C –this time for a significantly longer duration compared to the stationary procedure.

Similarly, the oscillating cold debonding process exhibited clear disadvantages. The cooling required 360 s, more than twice the duration of the stationary process, rendering it comparatively inefficient. Moreover, it did not provide any practical benefit over the stationary cold debonding method regarding process speed or thermal control. While the oscillating procedures yielded relatively uniform temperature distributions across the defined sections, the extended process times are not representative of realistic applications. In particular, the prolonged exposure to critical temperatures during warm debonding poses an additional risk to the integrity of the lower adhesive joint. Consequently, the subsequent section will concentrate on the stationary thermal application procedure pertinent to the debonding process itself, as it embodies a more practical and efficient methodology.

Mean temperature evaluation and process window analysis

To assess the thermal load acting across the adhesive flange during both warm and cold thermal applications, the average temperature variation over time was evaluated for the upper and lower adhesive layers (see Fig. 11). These values embody the spatially averaged temperatures obtained from all thermocouple readings along the bond line, thereby offering a comprehensive assessment of the overall thermal exposure throughout each procedure.

In the case of the analysed warm debonding method, the average temperature in the upper adhesive layer gradually increases and exceeds 100 °C after approximately 420 seconds. Simultaneously, the lower adhesive layer, though not directly exposed, surpasses the critical operating limit of 80 °C due to heat conduction and thermal inertia. This results in prolonged thermal load across the entire flange, including areas that are not intended to be debonded, posing a risk of thermal degradation or irreversible premature ageing. By contrast, the cold debonding method exhibits a rapid decrease in the average temperature of the upper adhesive layer, reaching sub-zero values within the first 30 seconds. Crucially, the average temperature in the lower adhesive layer remains well above the critical threshold of −40 °C throughout the process. This demonstrates that the cooling effect is confined to the intended bond line, without adversely affecting the surrounding joint area.

The comparison of both mean temperature curves clearly highlights the process-specific differences in energy input. While warm debonding results in a broad and prolonged temperature load across the entire flange, the cold method enables a faster, more localised, and minimally invasive thermal intervention. This targeted thermal management can support the preservation of adjacent structures, qualifying cold debonding as an approach for application-oriented, repair-capable separation processes with high potential for further investigation.

Life cycle assessment

The study was conducted using SimaPro software (Release 9.4.0.2) and the Ecoinvent 3.0 database. The software enables both the creation of individual data sets to replicate the analysed processes and the detailed analysis of contributing categories.

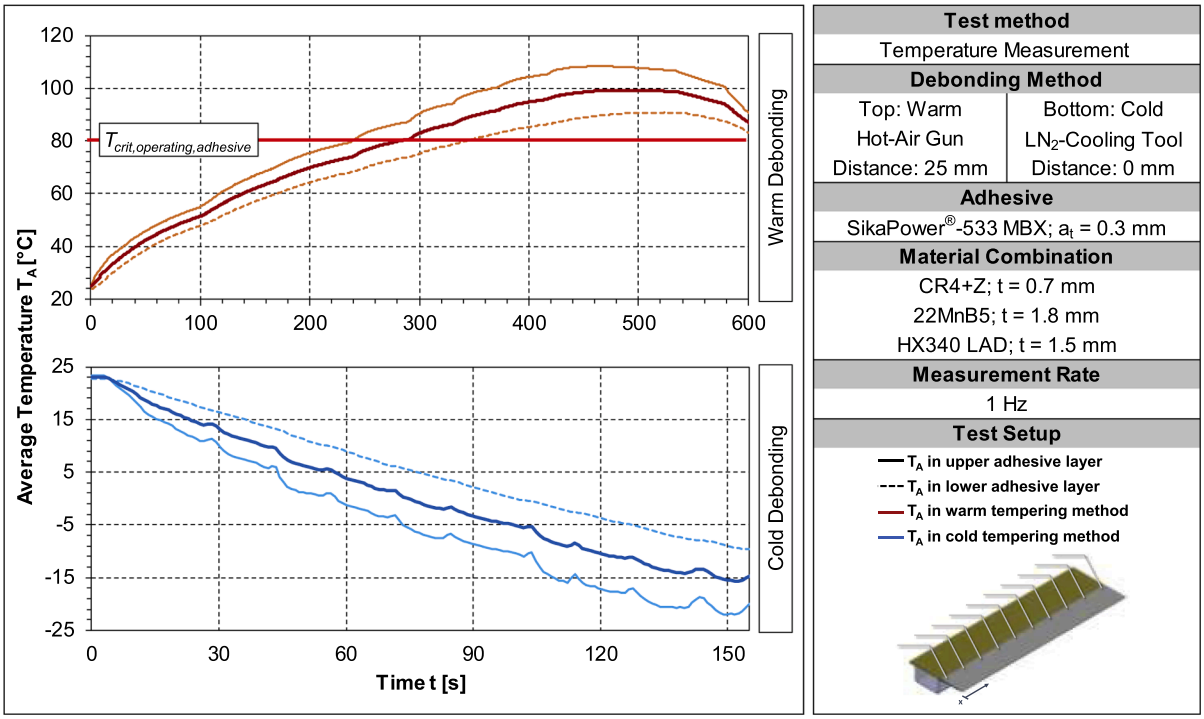

Fig. 11. Process-induced average temperature changes within the adhesive layers.

Goal and scope

Goal

The objective of the LCA is to scientifically analyse the environmental factors and impacts associated with the investigated debonding methods using a triple-layer adhesive joint, representative of a structural connection in automotive body-in-white construction. The results aim to support the evaluation of the methods based on relevant technological and environmental indicators and to identify potential for resource-efficient process optimisation within debonding operations.

Currently, ecological, social, and economic aspects are increasingly assessed across the entire life cycle of joined products and integrated into product development and customer consultation, as demonstrated by the example of the Arnold-Group (Bose-Munde 2024). However, a comprehensive evaluation and objective comparison of different debonding technologies and processes remains constrained due to a lack of available data. Nevertheless, suitable debonding technologies are highly relevant for adhesive bonding. They are considered enablers to improve the contribution of adhesive joints to the R-strategies of the EU Waste Framework Directive, specifically, Repair (R4), Refurbish (R5), Remanufacture (R6), Repurpose (R7), and ultimately to Recycling (R8) (Directorate-General for Environment 2023).

The findings of this study are addressed to both public and private research institutions to encourage further scientific and application-oriented research aimed at expanding the state of knowledge and facilitating industrial implementation. In addition, the study is intended to raise awareness within the industry, promote the integration of LCA into R&D processes, support the transfer of methods and know-how for internal implementation, and contribute to the development of innovative and resource-efficient products. Ultimately, this work seeks to provide guidance for the ecological evaluation of debonding technologies in a defined application scenario and to identify current research gaps in this field.

In order to assess the environmental impacts of actions and technologies, so called impact factors have to be chosen out of list. All of them have been assigned a unit in form of a reference substance. Other substances or gases than the unit can be more or less impactful in a certain period of time. For the scope and purpose of this journal, these five categories are chosen:

- Global warming potential (GWP) allows to measure the impact of greenhouse gases on global warming. The reference substance is carbon dioxide (CO_2) with 100 years as an often-used period of time (EPA 2025)
- Stratospheric ozone depletion potential (ODP) expresses the potential for damaging the ozone layer with the reference substance trichlorofluoromethane (CFC11, also known as R-11).
- Ozone formation expresses the risk of high levels of ground-level ozone on human health, by causing respiratory problems and exacerbating conditions such as asthma. The reference substance is nitrogen dioxide (NO_x)
- Fine particulate matter formation refers to the concentration of very small particles in the air that can penetrate deep into the lungs and cause respiratory and cardiovascular problems Reference substances are often particles with a diameter of up to 10 or 2.5 $^{\mu m}$. In this study, the latter was chosen, expressed as PM2.5.
- Terrestrial acidification potential (AP) describes the harmful effect on terrestrial ecosystems caused by a decrease in soil pH with the reference substance sulfur dioxide (SO_2).

Scope

The production processes under investigation encompass both a manual warm and a cold debonding method for separating 0.5 m of a structural adhesive joint within a component-representative specimen geometry replicating the functional composition of structural body-in-white assemblies. Accordingly, the assessed process serves the general function of separating two structurally bonded components to facilitate either the repair of a damaged part or the reintegration of materials into the circular economy.

The study is conducted using a gate-to-gate system boundary. Official input datasets from the Ecoinvent 3.0 database are employed to account for raw materials and subprocesses not directly measured during testing. This ensures the inclusion of relevant system inflows and outflows that fall outside the defined measurement scope. The system boundaries of the analysed processes are illustrated in Fig. 12. They encompass all subprocesses, equipment, and devices required to perform

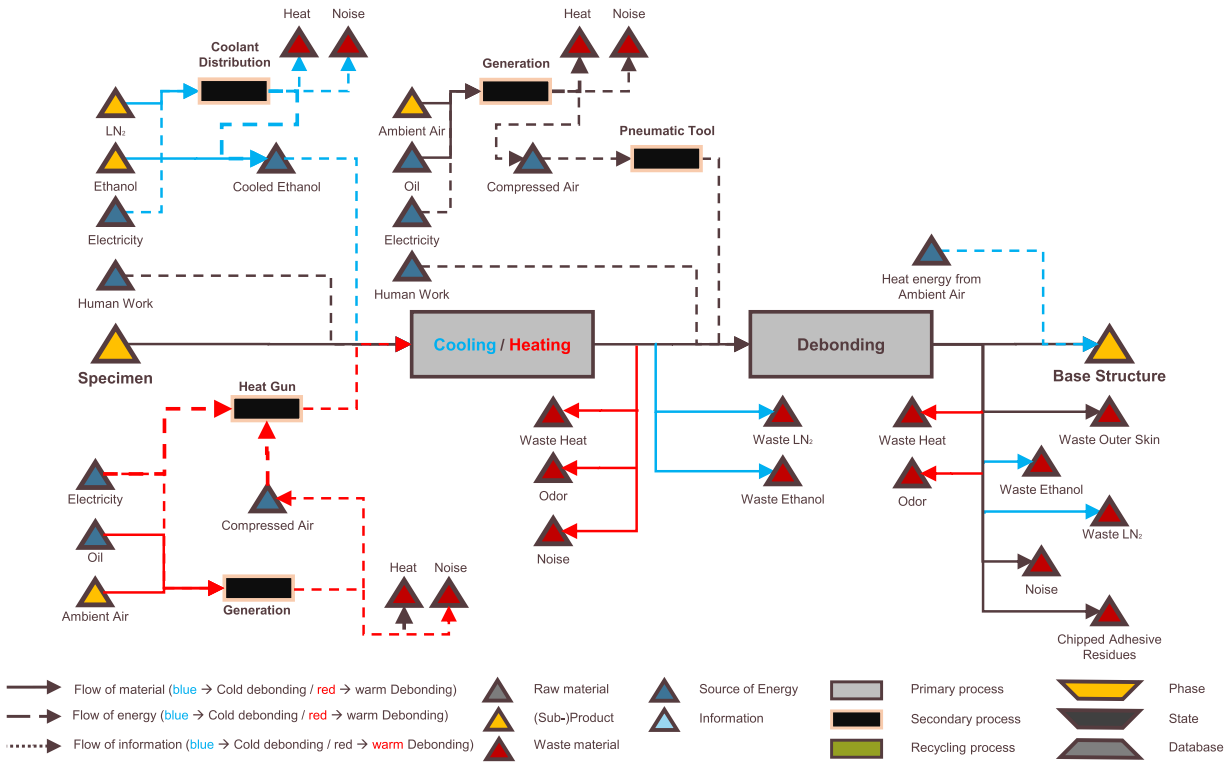

Fig. 12. Process definition and analysis of the system element flows for the cold method.

the debonding operations, as well as to generate or convert the necessary energy carriers. Only directly attributable foreground processes within the debonding workflow are considered. The production and EoL-disposal of machinery, along with indirect background processes such as administration or planning, are excluded due to the lack of reliable laboratory-scale datasets.

It is worth noting that the operational phase of debonding tools accounts for the largest share of environmental impact over its lifecycle –approximately 57.2 % (Shi et al. 2021). The choice of processing technology (Narita et al. 2009), the energy source and consumption (Santos et al. 2011), and the specific process parameters (Shi et al. 2021) significantly influence the ecological burden of machine use. Machine production accounts for an estimated 40 % of the environmental impact (Santos et al. 2011). The recyclability of machine components is a key factor for the environmental performance at EoL. Suitable recycling strategies have the potential to reduce emissions by up to 194 t CO_2 eq. per machine (Yan et al. 2024).

To evaluate the recoverable materials from the debonded components in both repair and recycling scenarios at EoL, official output datasets from the aforementioned database are used. A contribution threshold of at least 1 % of total emissions was defined as a cut-off criterion for outputs to maintain sufficient clarity in the system model.

Allocation of relevant and indirectly attributable elementary flows is based on mass fractions. Time-dependent flows, such as human labour, are allocated according to their share of time within the process. All accessible datasets are used in a consistent manner, following the "allocation, cut-off by classification" system model to assign responsibility for co-occurring emissions and waste to the respective organisational unit. For impact assessment and interpretation, the impact categories were analysed using the ReCiPe 2016 v1.07 method, as midpoint indicators like GWP are currently the standard for product evaluations by manufacturers. Method selection was guided by the ILCD Handbook (Joint Research Centre 2010) and aligned with the recommendations in Guinée et al. (2002). The data sources used include internal processes represented in high resolution by directly recorded input and output flows. Primary data was collected directly from the process, secondary data was derived indirectly, and tertiary data was assigned to the respective process modules through allocation. External processes are treated as black boxes and integrated using appropriate primary literature. All identified subprocesses include a comprehensive capture of associated inputs and outputs. The use of objective measurement data and widely accepted, publicly available databases ensures a transparent and reproducible assessment of the investigated system. The specific data requirements applied are listed in Table 3.

Within the scope of this study, the authors acknowledge limitations regarding the accuracy and validity of the data. Higher-level background processes are not fully represented due to the defined system boundaries, cut-off criteria, and the restriction to directly attributable elementary flows. Furthermore, the results depend on the investigated demonstrator and the mass shares of its individual components, which introduces a bias and leads to an underestimation of the overall environmental impact of the evaluated process.

Table 3
Data requirements within the assessment.

Time-based scope of coverage	< 10 years (after 2011)
Geographical scope of coverage	Germany > Europe
Technological scope of coverage	State of the art
Precision	Variance < 10 %
Integrity	> 90 %
Representativity	The scope is covered due to the closed view of the production processes within a company.
Consistency	Consistency is ensured in all data collection and analysis processes due to the consistent application of the principles outlined in this report.
Reproducibility	Reproducibility is accomplished due to multiple reference measurements.
Uncertainties	Shared processes, mass scaling to derive ecological indicators for other products, transferability to other systems, transferability to other production processes.

To assess the influence of data quality and methodological choices on the results of the environmental assessment, an uncertainty analysis was conducted. Uncertainty factors, as described by Ciroth et al., 2016, were determined using the pedigree matrix, based on data origin. This included the categories of reliability, completeness, temporal correlation, geographical correlation, and further technological correlation, rated on a five-point scale, in conjunction with a basic uncertainty factor. The resulting quantitative uncertainty factors were processed in a Monte Carlo simulation using 1000 iterations and a 95 % confidence interval. The resulting probability distribution was then used to verify the variability and uncertainty of the calculated assessment results.

Additionally, a sensitivity analysis was conducted to assess the impact of key assumptions on the results. In this context, process times were varied by 20 % to assess the effect of deviations in labour time. Such deviations can result from various influencing factors. According to Koruca et al. (2024), the learning curve significantly affects process times during the first 60 to 90 working days. Further deviations of up to 2.1 % may be attributed to the time of day of the work shift, up to 5 % to worker fatigue due to shift duration, and up to 3 % to unforeseen process disturbances. Other influencing factors include product mix, process stability, equipment availability, and material logistics. In this context, reduced production rates have been shown to result in average capacity losses of between 9 % and 15 % across different industry sectors (Tattner et al. 2020). Typically, deviations of 5 % to 20 % are defined to capture the relevant factors in sensitivity analyses. Based on the identified uncertainties in the measurement data, a broader variation range was selected to avoid underestimating process sensitivity. These findings assist the authors in estimating which deviations in partially subjective process times can be expected under real-world conditions and enable the identification of further efficiency potentials through improved training or reduced cycle times via targeted measures.

Collection of data

Data collection was conducted through the measurement of the identified elementary flows during the debonding experiments for the two methods under investigation. Electrical energy consumption was recorded in accordance with IEC 61000–4–30 Class A standards. For this purpose, a Fluke 435 Series II power quality analyser was employed (Fluke Corporation 2024). Phase voltages and line-to-neutral voltages were obtained via direct connections to the power supply line, while the individual and total currents for conductors L1, L2, L3, and the neutral line were measured using current clamps.

The debonding experiments were fully recorded on video. Process times were determined through manual evaluation of the video and audio tracks. For this purpose, the process duration was defined as the period from the start of the heating or cooling phase to the complete detachment of the cover sheet. Compressed air consumption was calculated based on the laboratory network system pressure and the measured process time. Network pressure and any potential pressure drops during testing were monitored and verified using a parallel-connected barometer. LN_2 consumption was determined from the sensor-recorded flow rate and the respective process duration. For this, the system was initially flushed at 100 % delivery capacity. During the experiments, a constant volumetric flow corresponding to 50 % delivery rate was maintained. The correlation between set and actual LN_2 delivery was verified in preliminary trials. The amount of ethanol applied was determined by gravimetric differential weighing before and after the process.

Life cycle inventory (LCI)

Within the LCI, process data were identified according to the previously defined requirements based on the conducted debonding experiments. The mean values and standard deviations of material and energy flows for the investigated debonding processes are summarised in Table 4. These values were calculated from five reproducible test runs for each method.

The recorded process data indicate increased electricity consumption for warm debonding, attributed to the energy-intensive heating process. Furthermore, the data suggest a reduced debonding effort in the case of cold debonding. The experiments show both a shorter overall and active debonding time, alongside lower compressed air consumption for the chisel, resulting from the reduced debonding work required to separate the adhesive layer. In contrast, cold debonding involves the use of process media that are emitted into the atmosphere, potentially impacting air quality.

Results –life cycle assessment

The examined processes were modelled using suitable individual process templates within the SimaPro framework, based on the measured data sets.

The dataset for electricity (Market for electricity, medium voltage {DE} | Cut-off, U) includes electricity inputs both produced in Germany and from imports as well as the transformation to medium voltage, the transmission network, direct emissions to air, and electricity losses during transmission. However, it does not include the electricity losses during the transformation from high to medium voltage, the leakage of insulation oil from cables, and electrotechnical equipment (Ecoinvent 2024). In the data set for compressed air (Market for compressed air, 600 kPa gauge {RER} | Cut-off, U), all activities were considered from the provision of compressed air generated by different technologies to the supply of a market mix of compressed air to the customer. An external supply of compressed air was therefore assumed. The assessment of required human working time (undefined work, human {DE} | Cut-off, U) may be applied to determine the human share in industrial processes. An average CO_2-eq. of 10.80 tons per year was assumed for a German citizen (German Federal Environment Agency 2023). A scaling factor of 5.5559 results in an average annual working time of 1587.8 h a year and the ratio of working time to total life of an average employee (Statista Research Department 2024). A complete emission of the process agents into the ambient air was assumed for the consumed volume of ethanol and nitrogen. The impact of direct emissions in the process was considered by the Emissions to Air process in the Life Cycle Impact Assessment (LCIA) phase. The modelled processes were subsequently utilised to assess the potential impacts in the LCIA phase.

Table 4
Measured mean values and standard deviations of material and energy flows in the investigated debonding processes.

		Unit	Warm Debonding		Cold Debonding	
			Mean	Standard Deviation	Mean	Standard Deviation
Heating / Cooling	**Ethanol**	Volume in l	–	–	0.011	0.001
	Nitrogen	Volume in l	–	–	0.174	0.016
	Electricity	Energy in Wh	91.464	14.641	0.813	0.111
	Compressed Air	Volume in Nm^3	0.549	0.083	–	–
	Human Work	Time in s	134.800	21.564	78.275	8.211
Debonding	**Compressed Air**	Volume in Nm^3	0.558	0.026	0.249	0.043
	Human Work	Time in s	89.800	14.366	53.275	5.589

Warm debonding

Table 5 presents the results of the LCIA phase for the warm debonding process. The process, involving temperature elevation followed by mechanical separation of the adhesive bond, is associated with total emissions of 0.559 kg CO_2-eq. in the impact category Global warming.

Fig. 13 illustrates the contributions of the investigated material and energy flows to the impact categories defined by the ReCiPe 2016 V1.07 method for the warm debonding process. The total emissions in the global warming category amount to 0.559 kg CO_2-eq., of which 62.41 % are attributable to the heating phase and 37.59 % to the subsequent mechanical separation process. Manual operations during heating (47.41 %) and debonding (31.66 %) contribute most significantly to the total impact. In contrast, electrical energy (9.19 %) and compressed air (11.74 %) account for a comparatively small share of emissions within the debonding process. As a result, the environmental impact is primarily driven by process duration, which could be reduced by increasing heating power and optimising thermal transfer from the heating device to the adhesive joint.

In the assessment of further impact categories, a more balanced contribution is observed between electrical energy and compressed air consumption during heating, and the compressed air required for mechanical separation. Contrary to the distribution seen in the global warming category, the compressed air consumption during the overall process exerts a notably greater influence on the remaining impact categories. Therefore, improving the environmental performance of the warm debonding process can be achieved by reducing process time and by switching to carbon-neutral electricity and fully electric devices for both heating and adhesive separation.

Cold debonding

For the cold debonding process, the LCIA conducted results in a total impact of 0.337 kg CO_2-eq. Of this, 0.216 kg CO_2-eq. (64.36 %) is attributed to the cooling phase, and 0.120 kg CO_2-eq. (35.64 %) to the subsequent mechanical separation of the adhesive bond. Total emissions in the global warming impact category are therefore approximately 39.89 % lower compared to the warm debonding process. The results for the remaining impact categories are summarised in Table 6.

The overall contribution of manual operations during cooling (45.83 %) and debonding (31.25 %) to emissions in the cold debonding process, as shown in Fig. 14, is comparable to that observed for the warm debonding method. Electrical energy (0.14 %) and compressed air (4.38 %) represent only a minor share of total emissions. The process media used, nitrogen (9.34 %) and ethanol (9.06 %), not only affect the GWP but also exhibit significant negative impacts in the category Ozone formation, human health (86.5 %). As nitrogen oxide equivalents are the reference substances for these categories, the emitted nitrogen is identified as the principal contributor. Implementing exhaust systems to capture process gases could therefore help reduce emissions during the debonding operation. Furthermore, material consumption could be lowered through automation and improved process parameterisation. This would also lead to reduced process durations, consequently enhancing the environmental performance of the cold debonding process.

Ecological comparison

Fig. 15 summarises the LCIA results for the investigated debonding processes and compares the normalised impacts of both methods across the different impact categories chosen. In this comparison, the higher maximum value within each impact category is used as the reference value for normalisation.

The results clearly show the lower impact of the cold debonding method in the categories GWP and fine particulate matter formation. In case of the acidification potential, this method shows slightly lower values than the warm debonding. For ozone depletion and ozone formation warm debonding is clearly in advantage and has a much lower impact.

Uncertainty and sensitivity analysis

An uncertainty analysis and a sensitivity analysis were subsequently performed to assess the impact of uncertainties within the study. The results in Table 7 enable the verification of uncertainties within the collected direct and indirect primary and secondary data, as well as the cut-off and allocation rules, assumptions, and methods for impact assessment described and employed in the study.

The ascertained standard deviation and variance in the results are particularly attributable to the uncertainties within the data used. Data sets with a different geographical correlation were used if no data records were available for processes in Germany. These include consumables such as ethanol (Europe), LN_2 (Europe), and compressed air (Europe). The increased variance in the debonding processes can further be attributed to the integration of subjective manual work steps. The average cycle times were measured and assigned a correspondingly higher uncertainty, as these values depend predominantly on the experience of the employees as well as their physical condition and level of concentration.

Subsequently, a sensitivity analysis was performed to assess the subjective share of manual work steps in the debonding process. For this purpose, the required process time for the individual work steps was varied both upwards and downwards. This study aims to assess both measurement inaccuracies and the impact of various work experiences and rates on the process flows that have the most significant influence on the LCIA result in the global warming impact category. Within the sensitivity analysis, three scenarios were created to represent the different work situations. Scenario 1 represents the standard process already investigated in Sections 4.3.1 to 4.3.3. Scenario 2 assumes 20 % shorter manual working times, and Scenario 3 assumes 20 % longer manual working times. The results of the sensitivity analysis are shown in Table 8. According to the DIN EN ISO 14044 (ISO 2021b) standard, the sensitivity analysis results are considered significant when they are above 10 %. The results are significant if the process has a sufficiently high contribution to the overall impact.

The results show a significant contribution of the human work steps in both Debonding processes. Thus, a reduction or increase in manual working time can result in an almost equivalent change in the impact on the global warming category by a factor of 0.6. The result implies a significant reduction in emissions within the investigated impact category as a result of increasing automation and the parallel reduction in cycle time.

Table 5
Ecological impacts of the investigated material and energy flows for the warm debonding process to the assessed impact categories.

Impact Category	Unit	Heating			Debonding	
		Electricity	Compressed Air	Human Work	Compressed Air	Human Work
Global warming	kg CO_2-eq.	5.14E-2	3.25E-2	2.65E-1	3.30E-2	1.77E-1
Stratospheric ozone depletion	kg CFC_{11}-eq.	2.67E-8	1.56E-8	–	1.59E-8	–
Ozone formation, human health	kg NO_x-eq.	5.22E-5	6.09E-5	–	6.19E-5	–
Fine particulate matter formation	kg $PM_{2.5}$-eq.	2.55E-5	5.31E-5	–	5.40E-5	–
Terrestrial acidification	kg SO_2-eq.	7.52E-5	1.33E-4	–	1.35E-4	–

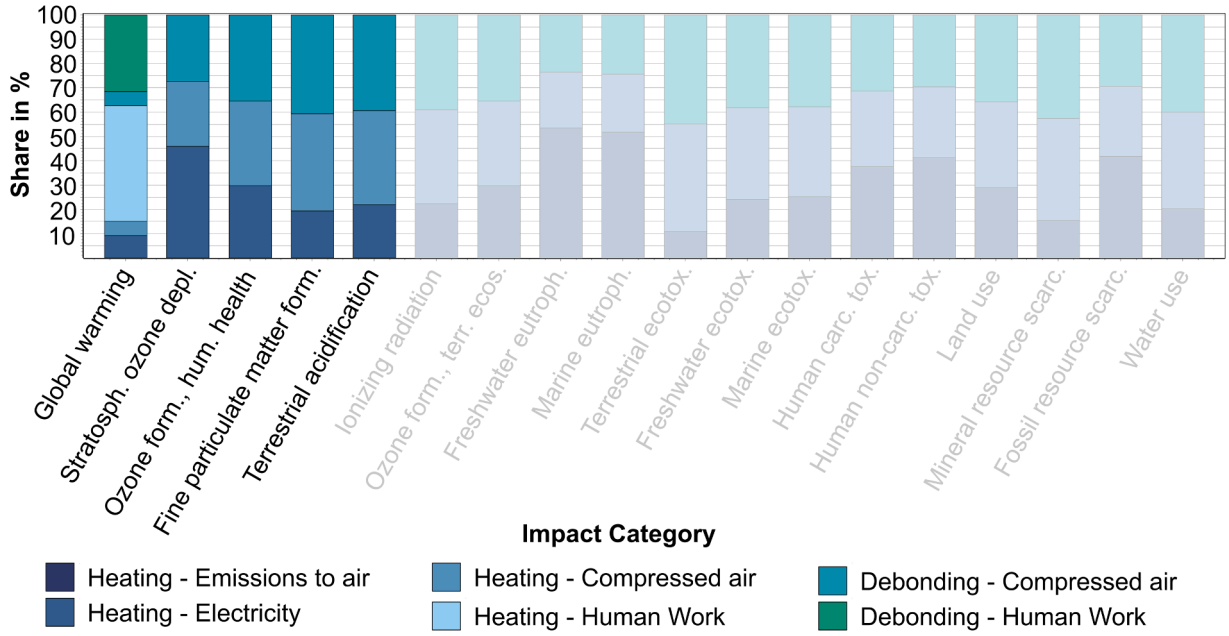

Fig. 13. Contributions of the investigated material and energy flows for the warm debonding process to the assessed impact categories.

Table 6
Ecological Impacts of the Investigated Material and Energy Flows for the Cold Debonding Process to the Assessed Impact Categories.

Impact Category	Unit	Cooling				Debonding		
		Ethanol	Nitrogen	Emissions to Air	Electricity	Human Work	Compressed Air	Human Work
Global warming	kg CO_2-eq.	3.04E-2	3.14E-2	–	4.57E-4	1.54E-1	1.47E-2	1.05E-1
Stratospheric ozone depletion	kg CFC_{11}-eq.	2.70E-7	1.52E-8	–	2.37E-10	–	7.08E-9	–
Ozone formation, human health	kg NO_x-eq.	8.45E-5	5.87E-5	1.10E-3	4.64E-7	–	2.76E-5	–
Fine particulate matter formation	kg $PM_{2.5}$-eq.	4.31E-5	4.66E-5	–	2.27E-7	–	2.41E-5	–
Terrestrial acidification	kg SO_2-eq.	1.60E-4	1.17E-4	–	6.68E-7	–	6.02E-5	–

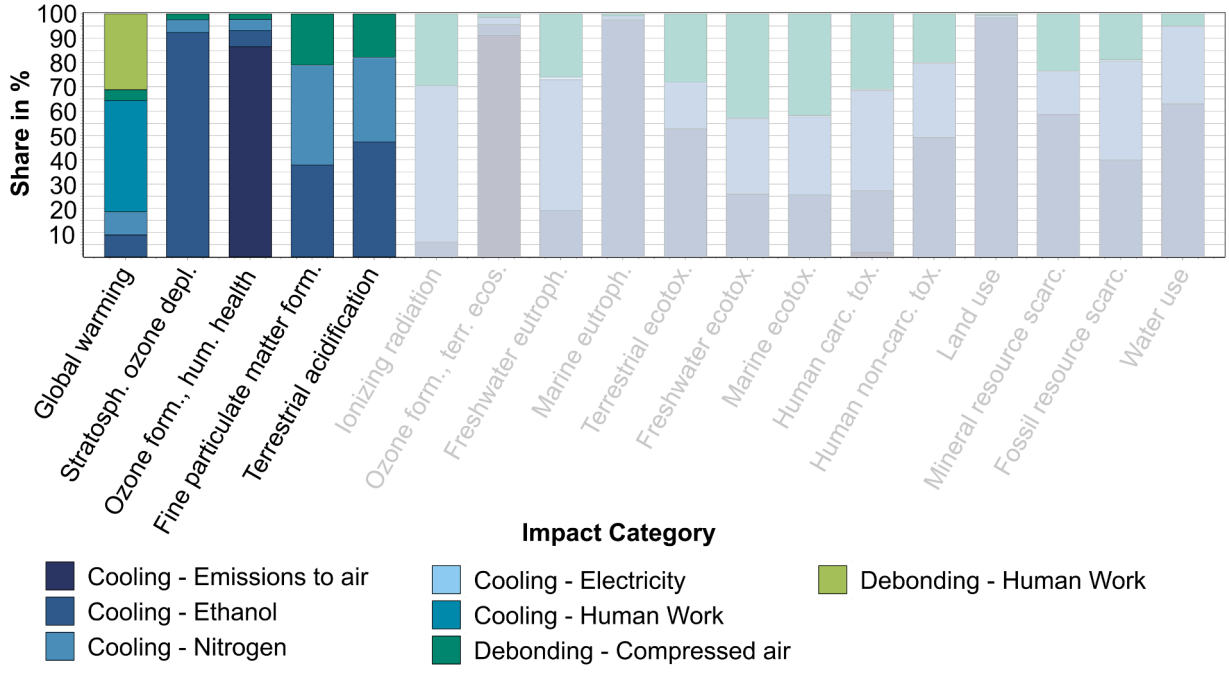

Fig. 14. Contributions of the investigated material and energy flows for the cold debonding process to the assessed impact categories.

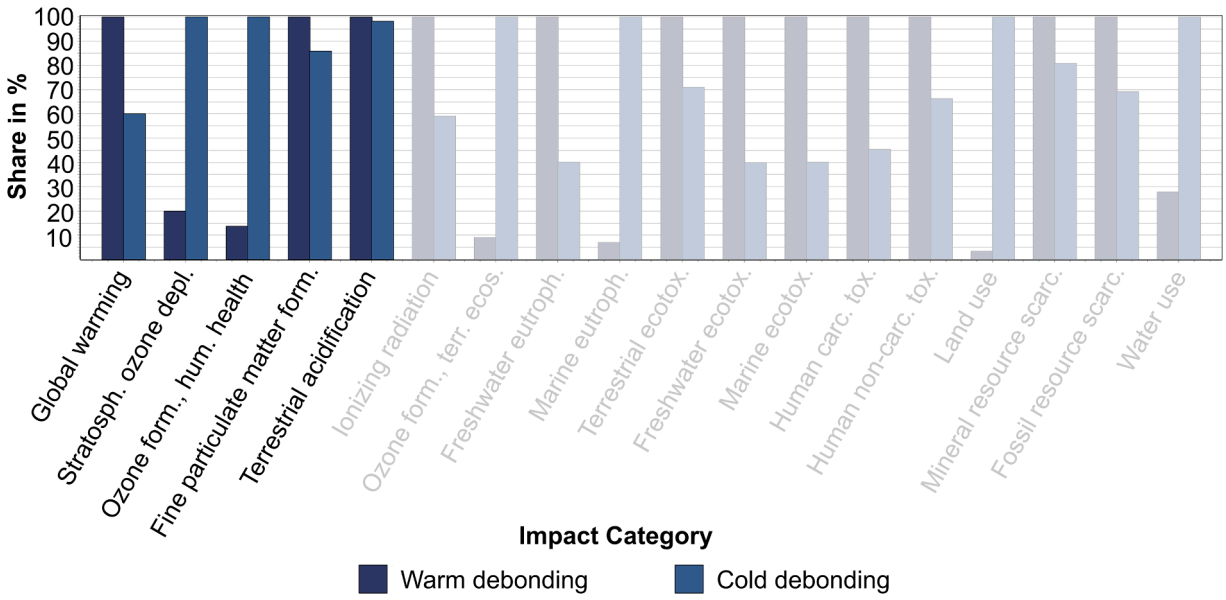

Fig. 15. Normalised impact of the investigated debonding methods across the impact categories based on the maximum reference value.

Table 7
Uncertainty analysis based on the results for GWP of the investigated debonding processes.

Process	Mean	Standard deviation	Unit	Variance
Warm Debonding	0.554	0.135	kg CO_2-eq.	24.40 %
Cold Debonding	0.337	0.079	kg CO_2-eq.	23.30 %

Table 8
Sensitivity analysis based on the results for GWP of the investigated debonding processes.

Process	Scenario 1	Scenario 2	Scenario 3	Unit	Reduction / Increase
Warm debonding	0.559	0.488	0.630	kg CO_2-eq.	-/+ 12.70 %
Cold debonding	0.336	0.294	0.378	kg CO_2-eq.	- /+ 12.50 %

Discussion

The presented findings enable a comprehensive evaluation of the two investigated debonding methods, hot-air-based warm debonding and cryogenic cold debonding, in terms of their process performance, structural impact, and environmental potential. While certain aspects of the discussion were introduced in Section 3 to support the interpretation of the results, the following section offers a more thorough discussion, including the environmental assessment from Section 4.

Process reproducibility

The general reproducibility of the recorded temperature profiles and process durations confirms the robustness of the experimental setup and demonstrates the methodological suitability of both the applied test procedures and the debonding processes, regardless of their current TRL. Particularly for the cold method, low deviations in temperature gradients and process times indicate high process consistency. In contrast, the warm method exhibits significantly higher variability, primarily due to the indirect convective heat transfer and its sensitivity to ambient conditions. For repair applications under real-world conditions, where predictability and repeatability are essential, cold debonding, as investigated here using the selected tools and setups, better fulfills key requirements for reliable process execution.

Mechanical integrity of adjacent adhesive layers in the re-use case

The evaluation of the l-tensile specimen does not reveal significant discrepancies in the mechanical behavior of the adjacent adhesive layer following the debonding process. Despite the considerable number of specimens that were examined, no clear correlation was identified between the debonding method employed and the resulting total deformation energy, when compared with the reference. The results demonstrated a relatively high standard deviation for all groups tested, which was attributed to the uncontrolled amount of adhesive used and the subsequent squeeze-out. However, the standard deviation from the warm-method was double that of the standard deviation from the cold-method. While this finding suggests a potential impact of the debonding method on the predictability of the adjacent adhesive layer, the study did not provide sufficient evidence to substantiate this hypothesis. Consequently, the impact of thermal-based debonding methods on the mechanical properties of the adjacent adhesive layer must be investigated further in separate studies.

Environmental impact and process efficiency

The results of the LCA clearly favour cold debonding in terms of GWP. Despite the use of LN_2 and ethanol, the GWP for cold debonding amounts to only 0.337 kg CO_2-eq., which is approximately 40 % lower than the 0.559 kg CO_2-eq. of warm debonding. This reduction is primarily due to lower energy consumption and shorter process durations. The warm method, by contrast, is characterised by a high demand for heating energy and manual input, both of which significantly contribute to overall process costs and emissions.

Nevertheless, certain impact categories, such as stratospheric ozone depletion and ozone formation, exhibit higher contributions for the cold method. These are mainly driven by emissions of evaporated process media. Mitigation strategies such as process gas capture systems, improved equipment design, or substituting ethanol with low-GWP cryo-stable media could help reduce these effects. Overall, cold debonding offers greater potential for optimisation and automation, which in turn would further enhance its environmental performance.

Holistic process evaluation

By combining the technical findings with the environmental assessment, the present study demonstrates that cold debonding offers clear advantages in terms of structural compatibility, reproducibility, and sustainability. Especially for repair-oriented use cases, where the preservation of components and the integrity of remaining joints are prioritised, this method enables a precise, minimally invasive, and thermally gentle separation. While this study employed pneumatic chiselling as the mechanical separation method for both debonding approaches, the environmental advantage of cold debonding is expected to remain consistent with alternative mechanical loading techniques. Since the LCA comparison was conducted using identical mechanical separation methods for both thermal approaches, the observed global warming potential ratio is primarily driven by the thermal conditioning phase rather than the mechanical separation process. Since both methods demonstrate effectiveness for the investigated material combination and geometry, their applicability is inherently limited by geometric accessibility and material-specific constraints. The requirement for direct contact in cold debonding may restrict its use in complex joint geometries, whereas the convective heating approach offers greater accessibility advantages in confined spaces. Here, the further development of the cooling tool is a valuable approach for further investigations and possible optimisations.

At the same time, it is essential to differentiate between the repair and recycling use cases. While material integrity is crucial in repair applications, it becomes secondary in recycling contexts. Here, the focus is on complete disassembly and material separation to enable high-purity material recovery. In such cases, the high thermal exposure observed in warm debonding may be acceptable or even desirable to facilitate the separation process. Therefore, it can be concluded that cold debonding is preferable for component- and function-oriented applications, whereas warm debonding remains a viable solution for material-oriented end-of-life strategies, particularly when factors such as technological simplicity, equipment availability, or lower process demands are prioritised.

Conclusion

This study presents a comprehensive analysis and evaluation of two physical debonding methods for structural adhesive joints: the conventional warm debonding using a hot air gun and the innovative cold debonding method based on a LN_2-cooled tool. The objective was not only to assess their thermal and mechanical effects on the bonded component but also to evaluate their environmental efficiency in the context of potential repair and recycling applications.

The experimental results reveal that the cold method offers significant advantages in terms of process duration and thermal selectivity. With an average debonding speed of 353.6 mm/min, cold debonding was approximately 49 % faster than the warm method, which achieved an average speed of 173.9 mm/min. This discrepancy can be attributed to the distinct physical mechanisms involved: while hot air transfers heat inefficiently to the component through convection, the LN_2-based tool removes heat more effectively and precisely through direct contact.

Differences in the thermal exposure of the lower, non-target adhesive layer were particularly pronounced. Whereas temperatures of 150–160 °C were reached during warm debonding, the temperature in the lower adhesive layer remained consistently above the critical threshold of −40 °C during cold debonding, thus staying within the functional range of typical structural adhesives. The average temperature profiles along the adhesive flange confirmed the higher thermal control in cold debonding, characterised by both a faster and more spatially confined thermal response. This enables more targeted processing with reduced thermal impact on adjacent structural areas.

In terms of the structural integrity of the remaining adhesive bond, cold debonding also demonstrated a clear advantage in terms of reproducibility. The l-tensile specimens, additionally extracted after the debonding process, showed low scatter and force levels comparable to the untreated reference, indicating minimal impact on the adhesive layer. In contrast, warm debonding resulted in twice as high standard deviation at a slightly lower average level of maximum force and total deformation energy, suggesting irreversible thermal damage due to the intense heat input. This phenomenon must be investigated further in a separate study.

The environmental assessment, conducted via LCA, also showed a differentiated picture. Despite the use of liquid nitrogen and ethanol, cold debonding yielded approximately 40 % lower carbon footprint for the warm method. This outcome is mainly attributed to the significantly lower energy consumption and shorter process duration. Nevertheless, cold debonding showed higher contributions in specific impact categories such as ozone formation and ozone depletion, largely due to emissions from process media. These can potentially be reduced through closed-loop systems or by substituting critical auxiliary materials, such as ethanol.

It is crucial to evaluate both methods in the context of their intended application. In repair scenarios, where the preservation of the remaining structure and adhesive bond is essential, LN_2-based cold debonding offers clear advantages. In contrast, for material-focused recycling objectives, where the complete separation of bonded materials is the priority, the warm method using hot air may remain a viable and practical alternative, particularly when infrastructure or technical requirements are limited.

In summary, LN_2-based cold debonding has been demonstrated to be a highly selective, process-reliable, and ecologically favourable method, particularly well-suited for the separation of bonded structures while effectively maintaining their functionality. The suitability of cold debonding for repair-oriented applications is clearly evidenced in this study. Conversely, the warm debonding method remains applicable in scenarios that impose lower structural or functional demands. It should be noted that this investigation exclusively examined warm debonding using a hot air gun. Other heating sources, such as induction heating or contact-based systems, were not considered and represent promising areas for future research. Both methods exhibit significant optimisation potential, especially through automation, enhanced energy efficiency, and the development of low-emission processes.

Declaration of generative AI and AI-assisted technologies in the writing process

During the preparation of this work the authors used Grammarly Pro in order to enhance linguistic variety and proficiency. After using this tool/service, the authors reviewed and edited the content as needed and take full responsibility for the content of the publication.

Funding

The research and development project 'Development of methods for the efficient disassembly of steel adhesive bonds' is supported and funded by the Research Association for Steel Application e. V., Düsseldorf, under the funding reference P 1604 / S0024/10285/23, using funds from the Steel Application Research Foundation, Essen. The responsibility for the content of this publication remains with the authors.

CRediT authorship contribution statement

Alex Jordan: Writing – review & editing, Writing – original draft, Visualization, Methodology, Investigation, Formal analysis, Data curation, Conceptualization. **Lucas Hermelingmeier:** Writing – original draft, Visualization, Methodology, Investigation, Formal analysis, Data curation, Conceptualization. **Julian Gilich:** Writing – original draft, Visualization, Methodology, Investigation, Formal analysis, Data curation, Conceptualization. **Gerson Meschut:** Supervision. **Marco De**

Santis: Investigation. **Alexander Schlüter:** Supervision.

Declaration of competing interest

The authors declare that they have no known competing financial interests or personal relationships that could have appeared to influence the work reported in this paper.

Data availability

Data will be made available on request.

References

Bader B., Türck E., Vietor T. (2019) Multi material design. A current overview of the used potential in automotive industries. In: Dröder K, Vietor T (eds) *Technologies For Economical and Functional Lightweight design. Zukunftstechnologien für den Multifunktionalen Leichtbau*. Springer Vieweg, Berlin, Heidelberg. https://doi.org/10.1007/978-3-662-58206-0_1.

Bandl, C., Kern, W., Schlögl, S., 2020. Adhesives for 'debonding-on-demand': triggered release mechanisms and typical applications. Int. J. Adhes. Adhes 99, 1–19. https://doi.org/10.1016/j.ijadhadh.2020.102585.

Banea, M.D., 2019. Debonding on demand of adhesively bonded joints: a critical review. Rev. Adhes. Adhes 7 (1), 33–50. https://doi.org/10.7569/RAA.2019.097304.

Bartley, A., Chudalla, N., Meschut, G., et al., 2023. Low temperature debonding of toughened structural adhesive joints: a new approach to repairs in the automotive industry. Int. J. Adhes. Adhes 126, 103486. https://doi.org/10.1016/j.ijadhadh.2023.103486.

Bevilacqua, M., Ciarapica, F.E., D'Orazio, A., et al., 2017. Sustainability analysis of friction stir welding of AA5754 sheets. Procedia. CIRP 62, 529–534. https://doi.org/10.1016/j.procir.2016.06.081.

Borges, C.S.P., Akhavan-Safar, A., Tsokanas, P., et al., 2023. From fundamental concepts to recent developments in the adhesive bonding technology: a general view. Discov. Mech. Eng 2 (8), 1–8. https://doi.org/10.1007/s44245-023-00014-7.

Bose-Munde A. (2024) Ensuring that joining technology is sustainable. https://www.americanindustrialmagazine.com/blogs/manufacturing/ensuring-that-joining-technology-is-sustainable, Assessed 02 May 2025.

Chudalla, N., 2024. Failure and Debondability of Structural Adhesive Bonds at Low Temperatures. Dissertation. Paderborn University. ISBN 978-3-8440-9690-3.

Ciroth, A., Muller, S., Weidema, B., et al., 2016. Empirically based uncertainty factors for the pedigree matrix in ecoinvent. Int. J. Life. Cycle. Assess 21, 1338–1348. https://doi.org/10.1007/s11367-013-0670-5.

Concord, A., 2021. *Debonding Technologies For Adhesive Bonded structures*. Dissertation. Brandenburgische Technische Universität Cottbus.

Curran M.A. (2017) Overview of *goal and scope definition in life cycle assessment*. In: Curran MA (ed) Goal and Scope Definition in Life Cycle Assessment (LCA Compendium –The Complete World of Life Cycle Assessment) 1:1–62. Springer, Dordrecht. https://doi.org/10.1007/978-94-024-0855-3.

da Silva, L.A., Espinosa, C., Chieragatti, R., et al., 2025. Functionalization of adhesive bonding to control on-demand disassembly of composite structures. Aerospace 12 (4), 1–17. https://doi.org/10.3390/aerospace12040269.

DIN, 2009. European Standard DIN EN 1465:2009. Adhesives –Determination of Tensile Lap-Shear Strength of Bonded Assemblies. Beuth publishing house, Berlin.

DIN, 2010. European Standard DIN EN 1464:2010. Adhesives –Determination of Peel Resistance of Adhesive Bonds –Floating Roller Method. Beuth publishing house, Berlin.

DIN, 2020. National Standard DIN/TS 54405:2020-12. Construction Adhesives - Guideline for Separation and Recycling of Adhesives and Substrates from Bonded Joints. Beuth publishing house, Berlin.

Directorate-General for Environment, 2023. Proposal for a targeted revision of the Waste Framework Directive. Gen. Publ. Assessed 13 June 2024.

Ditter, J., 2020. Method Development for Debonding Steel Adhesive Joints At Low Temperatures. Dissertation. Paderborn University. ISBN 978-3-8440-7530-4.

DVS, 2012. National Standard DVS 2519-2:2012. Kleben in der Karosserie-Reparatur. Dtsch. Verb. Schweiß. verwandte. Verfahr. e,. V. (DVS). Düsseld.

Ecoinvent (2024) Ecoinvent version 3.7.1. Available in the SimaPro software (Release 9.4.0.2). https://support.ecoinvent.org/ecoinvent-version-3.7.1. Accessed 17 June 2024.

EPA, 2025. United States Environmental Protection Agency. Underst. Glob. Warm. Potentials. https://www.epa.gov/ghgemissions/understanding-global-warming-potentials. Accessed 12 July 2025.

European Commission (2000) Directive 2000/53/EC of the European Parliament and of the Council of 18 September 2000 on end-of life vehicles. https://eur-lex.europa.eu/legal-content/EN/TXT/?uri=CELEX%3A32000L0053. Assessed 19 May 2025.

Favi, C., Moroni, F., Lutey, A.H., et al., 2021. LCA of laser surface activation and traditional pre-treatments for adhesive bonding of engineering polymers. Procedia. CIRP 98, 541–546. https://doi.org/10.1016/j.procir.2021.01.148.

Fluke Corporation, 2024. Fluke 434-II/435-II/437-II three-phase mains and power supply analyzer. Oper. man. Rev,. 1. https://www.fuke-direct.ca/pdfs/cache/www.fluke-direct.ca/fuke/power_quality_analyzer/435_ii/manual/fuke_435_ii_power_quality_analyzer_manual.pdf. Accessed 07 Mar 2024.

Gagliardi, F., Palaia, D., Ambrogio, G., 2019. Energy consumption and CO2 emissions of joining processes for manufacturing hybrid structures. J. Clean. Prod 228, 425–436. https://doi.org/10.1016/j.jclepro.2019.04.339.

Agency, German Federal Environment, 2023. What. are. aver. greenh. gas. emiss. pers. Ger.? https://www.umweltbundesamt.de/service/uba-fragen/wie-hoch-sind-die-treibhausgas.emis-sionen-pro-person. Assessed 16 April 2024.

Gialos, A.A., Zeimpekis, V., Alexopoulos, N.D., et al., 2018. Investigating the impact of sustainability in the production of aeronautical subscale components. J. Clean. Prod 176, 785–799. https://doi.org/10.1016/j.jclepro.2017.12.151.

Goodenough, J., Fitzgerald, A., Bean, K., et al., 2023. Reversible adhesives and debondable joints for fibre-reinforced plastics: characteristics, capabilities, and opportunities. Mater. Chem. Phys 299, 127464. https://doi.org/10.1016/j.matchemphys.2023.127464.

Guinée, J.B., Gorrée, M., Heijungs, R., et al., 2002. Handbook On Life Cycle assessment. Operational guide to the ISO standards. I: LCA in perspective. IIa: Guide. IIb: Operational annex. III: Scientific background. Kluwer Academic Publishers, Dordrecht. https://doi.org/10.1007/0-306-48055-7.

Heinzmann, C., Weder, C., de Espinosa, L.M., 2016. Supramolecular polymer adhesives: advanced materials inspired by nature. Chem. Soc. Rev 45 (2), 342–358. https://doi.org/10.1039/c5cs00477b.

Hohl, D.K., Weder, C., 2019. De)bonding on demand with optically switchable adhesives. Adv. Opt. Mater 7 (16), 1–25. https://doi.org/10.1002/adom.201900230.

Hotairtools, 2024. Entfernen von Klebstoffen mit Heißluft. Hot. Air. Tools. –Blog. https://hotairtools.com/blogs/news/entfernen-von-klebstoffen-mit-heissluft. Assessed: 19-May-2025.

Hutchinson, A., Liu, Y., Lu, Y., 2016. Overview of disbonding technologies for adhesive bonded joints. J. Adhes 93 (10), 737–755. https://doi.org/10.1080/00218464.2016.1237876.

Inutsuka, M., Kondo, M., Koita, T., et al., 2023. Electrical properties of adhesives designed for smart debonding by a pulsed discharge method. J. Adhes 1–15. https://doi.org/10.1080/00218464.2023-2167600.

ISO, 2021a. International Standard DIN EN ISO 14040:2006 + A1:2020. Environmental Management –Life Cycle Assessment –Principles and Framework. Beuth publishing house, Berlin.

ISO, 2021b. International Standard DIN EN ISO 14044:2006 + A1:2018 + A2:2020. *Environmental Management –Life Cycle Assessment –Requirements and Guidelines*. Beuth publishing house, Berlin.

Joint Research Centre (JRC), 2010. Institute for Environment and Sustainability (IES). ILCD Handbook: Analysis of Existing Environmental Impact Assessment methodologies For Use in Life Cycle Assessment. Publications Office of the European Union, Luxembourg.

Khripko D., Schlüter A., Rosano M., Hesselbach J. (2013) Product carbon footprint in polymer processing –A practical application. In: G. Seliger (Ed.), Proceedings of the 11th Global Conference on Sustainable Manufacturing - Innovative Solutions, ISBN: 978-3-7983-2609-5, 10.14279/depositonce-3753.

Koruca H.İ., Urgancı K.B., Gamoura S.C. (2024) The significance of Human performance in production processes: an extensive review of simulation-integrated techniques for assessing fatigue and workload. In: Şen Z, Uygun Ö, Erden C. (eds) *Advances in Intelligent Manufacturing and Service System Informatics. IMSS 2023. Lecture Notes in Mechanical Engineering*. Springer, Singapore. https://doi.org/10.1007/978-981-99-6062-0_51.

Leijonmarck, S., Cornell, A., Danielsson, C.-O., et al., 2011. Electrochemical characterization of electrically induced adhesive debonding. J. Electrochem. Soc 158 (10), 109–114. https://doi.org/10.1149/1.3622657.

Leijonmarck, S., Cornell, A., Danielsson, C.-O., et al., 2012. Electrolytically assisted debonding of adhesives: an experimental investigation. Int. J. Adhes. Adhes 32, 39–45. https://doi.org/10.1016/j.ijadhadh.2011.09.003.

Lu, Y., Broughton, J., Winfield, P., 2014. A review of innovations in disbonding techniques for repair and recycling of automotive vehicles. Int. J. Adhes. Adhes 50, 119–127. https://doi.org/10.1016/j.ijadhadh.2014.01.021.

Maciel, V.G., Bockorny, G., Domingues, N., et al., 2017. Comparative life cycle assessment among three polyurethane adhesive technologies for the footwear industry. ACS. Sustain. Chem. Eng 5, 8464–8472. https://doi.org/10.1021/acssuschemeng.7b02516.

Narita, H., Fujimoto, H., 2009. Analysis of environmental impact due to machine tool operation. Int. J. Autom. Technol 3 (1), 49–55. https://doi.org/10.20965/ijat.2009.p0049.

Sangwan, K.S., Herrmann, C., Egede, P., et al., 2016. Life cycle assessment of arc welding and gas welding processes. Procedia. CIRP 48, 62–67. https://doi.org/10.1016/j.procir.2016.03.096.

Santos, J.P., Oliveira, M., Almeida, G., et al., 2011. Improving the environmental performance of machine-tools: influence of technology and throughput on the electrical energy consumption of a press-brake. J. Clean. Prod 19 (4), 356–364. https://doi.org/10.1016/j.jclepro.2010.10.009.

Sato, C., Carbas, R.J., Marques, E.A., et al., 2021. Effect of disassembly on environmental and recycling issues in bonded joints. In: Adhesive Bonding, 2. Woodhead Publishing, Cambridge, pp. 407–436. https://doi.org/10.1016/B978-0-12-819954-1.00016-2.

Shi, J., Hu, J., Ma, M., et al., 2021. An environmental impact analysis method of machine-tool cutting units based on LCA. J. Eng. Technol 19 (5), 1192–1206. https://doi.org/10.1108/JEDT-06-2020-0247.

Shrivastavaa, A., Krones, M., Pfefferkorn, F.E., 2015. Comparison of energy consumption and environmental impact of friction stir welding and gas metal arc welding for aluminum. J. Manuf. Sci. Techn 9, 159–168. https://doi.org/10.1016/j.cirpj.2014.10.001.

Sika, 2011. Product Data Sheet –SikaPower®-533 MBX. Sika Automotive AG. Romanshorn CH.

Sridhar, L.M., Oster, M.O., Herr, D.E., et al., 2020. *Re*-usable thermally reversible crosslinked adhesives from Diels–Alder networks. Green. Chem 22 (24), 8669–8679. https://doi.org/10.1039/D0GC02938F.

Statista Research Department (2024) Average annual working hours per employee (full-time and part-time) in Germany from 2001 to 2023. https://de.statista.com/statistik/daten/studie/4047/umfrage/entwicklung-der-jaehrlichen-arbeitszeit-pro-erwerbstaetigen. Accessed 16 April 2024.

Statistisches Bundesamt (2018) Waste volume in Germany at 417.2 million tons in 2018. https://www.destatis.de/EN/Home/_node.html. Assessed 19 May 2025.

Stauber, R., 2007. Plastics in automotive engineering. ATZ. Worldw 109 (2–4). https://doi.org/10.1007/BF03224916.

Tattner, A., Hvam, L., Haug, A., 2020. Why slow down? Factors affecting speed loss in process manufacturing. Int. J. Adv. Manuf. Technol 106, 2021–2034. https://doi.org/10.1007/s00170-019-04559-4.

Tillman, A.-M., Ekvall, T., Baumann, H., 1994. Choice of system boundaries in life cycle assessment. J. Clean. Prod 2 (1), 21–29. https://doi.org/10.1016/0959-6526(94)90021-3.

Yan, H.E., Guo, F., Zhang, B., et al., 2024. Sustainability assessment during machining processes: evidence from the econ-environmental modelling. J. Clean. Prod 448, 141612. https://doi.org/10.1016/j.jclepro.2024.141612.

Yilbas, B.S., Shaukat, M.M., Afzal, A.A., et al., 2020. Life cycle analysis for laser welding of alloys. Opt. Laser. Technol 126, 106064. https://doi.org/10.1016/j.optlastec.2020.106064.

Zhong, Lieshuang, Guo, Zhiguang, 2017. Effect of surface topography and wettability on the Leidenfrost effect. *Nanoscale*. 9 19, 6219–6236. https://doi.org/10.1080/00218464.2016.1199963.